Study of $D^+ \to K^-\pi^+e^+\nu_e$

M. Ablikim,[1] M. N. Achasov,[9,f] X. C. Ai,[1] O. Albayrak,[5] M. Albrecht,[4] D. J. Ambrose,[44] A. Amoroso,[49a,49c] F. F. An,[1] Q. An,[46,a] J. Z. Bai,[1] R. Baldini Ferroli,[20a] Y. Ban,[31] D. W. Bennett,[19] J. V. Bennett,[5] M. Bertani,[20a] D. Bettoni,[21a] J. M. Bian,[43] F. Bianchi,[49a,49c] E. Boger,[23,d] I. Boyko,[23] R. A. Briere,[5] H. Cai,[51] X. Cai,[1,a] O. Cakir,[40a,b] A. Calcaterra,[20a] G. F. Cao,[1] S. A. Cetin,[40b] J. F. Chang,[1,a] G. Chelkov,[23,d,e] G. Chen,[1] H. S. Chen,[1] H. Y. Chen,[2] J. C. Chen,[1] M. L. Chen,[1,a] S. Chen Chen,[41] S. J. Chen,[29] X. Chen,[1,a] X. R. Chen,[26] Y. B. Chen,[1,a] H. P. Cheng,[17] X. K. Chu,[31] G. Cibinetto,[21a] H. L. Dai,[1,a] J. P. Dai,[34] A. Dbeyssi,[14] D. Dedovich,[23] Z. Y. Deng,[1] A. Denig,[22] I. Denysenko,[23] M. Destefanis,[49a,49c] F. De Mori,[49a,49c] Y. Ding,[27] C. Dong,[30] J. Dong,[1,a] L. Y. Dong,[1] M. Y. Dong,[1,a] S. X. Du,[53] P. F. Duan,[1] J. Z. Fan,[39] J. Fang,[1,a] S. S. Fang,[1] X. Fang,[46,a] Y. Fang,[1] L. Fava,[49b,49c] F. Feldbauer,[22] G. Felici,[20a] C. Q. Feng,[46,a] E. Fioravanti,[21a] M. Fritsch,[14,22] C. D. Fu,[1] Q. Gao,[1] X. L. Gao,[46,a] X. Y. Gao,[2] Y. Gao,[39] Z. Gao,[46,a] I. Garzia,[21a] K. Goetzen,[10] W. X. Gong,[1,a] W. Gradl,[22] M. Greco,[49a,49c] M. H. Gu,[1,a] Y. T. Gu,[12] Y. H. Guan,[1] A. Q. Guo,[1] L. B. Guo,[28] R. P. Guo,[1] Y. Guo,[1] Y. P. Guo,[22] Z. Haddadi,[25] A. Hafner,[22] S. Han,[51] X. Q. Hao,[15] F. A. Harris,[42] K. L. He,[1] X. Q. He,[45] T. Held,[4] Y. K. Heng,[1,a] Z. L. Hou,[1] C. Hu,[28] H. M. Hu,[1] J. F. Hu,[49a,49c] T. Hu,[1,a] Y. Hu,[1] G. M. Huang,[6] G. S. Huang,[46,a] J. S. Huang,[15] X. T. Huang,[33] Y. Huang,[29] T. Hussain,[48] Q. Ji,[1] Q. P. Ji,[30] X. B. Ji,[1] X. L. Ji,[1,a] L. W. Jiang,[51] X. S. Jiang,[1,a] X. Y. Jiang,[30] J. B. Jiao,[33] Z. Jiao,[17] D. P. Jin,[1,a] S. Jin,[1] T. Johansson,[50] A. Julin,[43] N. Kalantar-Nayestanaki,[25] X. L. Kang,[1] X. S. Kang,[30] M. Kavatsyuk,[25] B. C. Ke,[5] P. Kiese,[22] R. Kliemt,[14] B. Kloss,[22] O. B. Kolcu,[40b,i] B. Kopf,[4] M. Kornicer,[42] W. Kuehn,[24] A. Kupsc,[50] J. S. Lange,[24] M. Lara,[19] P. Larin,[14] C. Leng,[49c] C. Li,[50] Cheng Li,[46,a] D. M. Li,[53] F. Li,[1,a] F. Y. Li,[31] G. Li,[1] H. B. Li,[1] H. J. Li,[1] J. C. Li,[1] Jin Li,[32] K. Li,[13] K. Li,[33] Lei Li,[3] P. R. Li,[41] T. Li,[33] W. D. Li,[1] W. G. Li,[1] X. L. Li,[33] X. M. Li,[12] X. N. Li,[1,a] X. Q. Li,[30] Z. B. Li,[38] H. Liang,[46,a] J. J. Liang,[12] Y. F. Liang,[36] Y. T. Liang,[24] G. R. Liao,[11] D. X. Lin,[14] B. J. Liu,[1] C. X. Liu,[1] D. Liu,[46,a] F. H. Liu,[35] Fang Liu,[1] Feng Liu,[6] H. B. Liu,[12] H. H. Liu,[16] H. H. Liu,[1] H. M. Liu,[1] J. Liu,[1] J. B. Liu,[46,a] J. P. Liu,[51] J. Y. Liu,[1] K. Liu,[39] K. Y. Liu,[27] L. D. Liu,[31] P. L. Liu,[1,a] Q. Liu,[41] S. B. Liu,[46,a] X. Liu,[26] Y. B. Liu,[30] Z. A. Liu,[1,a] Zhiqing Liu,[22] H. Loehner,[25] X. C. Lou,[1,a,h] H. J. Lu,[17] J. G. Lu,[1,a] Y. Lu,[1] Y. P. Lu,[1,a] C. L. Luo,[28] M. X. Luo,[52] T. Luo,[42] X. L. Luo,[1,a] X. R. Lyu,[41] F. C. Ma,[27] H. L. Ma,[1] L. L. Ma,[33] M. M. Ma,[1] Q. M. Ma,[1] T. Ma,[1] X. N. Ma,[30] X. Y. Ma,[1,a] F. E. Maas,[14] M. Maggiora,[49a,49c] Y. J. Mao,[31] Z. P. Mao,[1] S. Marcello,[49a,49c] J. G. Messchendorp,[25] J. Min,[1,a] R. E. Mitchell,[19] X. H. Mo,[1,a] Y. J. Mo,[6] C. Morales Morales,[14] K. Moriya,[19] N. Yu. Muchnoi,[9,f] H. Muramatsu,[43] Y. Nefedov,[23] F. Nerling,[14] I. B. Nikolaev,[9,f] Z. Ning,[1,a] S. Nisar,[8] S. L. Niu,[1,a] X. Y. Niu,[1] S. L. Olsen,[32] Q. Ouyang,[1,a] S. Pacetti,[20b] Y. Pan,[46,a] P. Patteri,[20a] M. Pelizaeus,[4] H. P. Peng,[46,a] K. Peters,[10] J. Pettersson,[50] J. L. Ping,[28] R. G. Ping,[1] R. Poling,[43] V. Prasad,[1] M. Qi,[29] S. Qian,[1,a] C. F. Qiao,[41] L. Q. Qin,[33] N. Qin,[51] X. S. Qin,[1] Z. H. Qin,[1,a] J. F. Qiu,[1] K. H. Rashid,[48] C. F. Redmer,[22] M. Ripka,[22] G. Rong,[1] Ch. Rosner,[14] X. D. Ruan,[12] V. Santoro,[21a] A. Sarantsev,[23,g] M. Savrié,[21b] K. Schoenning,[50] S. Schumann,[22] W. Shan,[31] M. Shao,[46,a] C. P. Shen,[2] P. X. Shen,[30] X. Y. Shen,[1] H. Y. Sheng,[1] M. Shi,[1] W. M. Song,[1] X. Y. Song,[1] S. Sosio,[49a,49c] S. Spataro,[49a,49c] G. X. Sun,[1] J. F. Sun,[15] S. S. Sun,[1] X. H. Sun,[1] Y. J. Sun,[46,a] Y. Z. Sun,[1] Z. J. Sun,[1,a] Z. T. Sun,[19] C. J. Tang,[36] X. Tang,[1] I. Tapan,[40c] E. H. Thorndike,[44] M. Tiemens,[25] M. Ullrich,[24] I. Uman,[40b] G. S. Varner,[42] B. Wang,[30] D. Wang,[31] D. Y. Wang,[31] K. Wang,[1,a] L. L. Wang,[1] L. S. Wang,[1] M. Wang,[33] P. Wang,[1] P. L. Wang,[1] S. G. Wang,[31] W. Wang,[1,a] W. P. Wang,[46,a] X. F. Wang,[39] Y. D. Wang,[14] Y. F. Wang,[1,a] Y. Q. Wang,[22] Z. Wang,[1,a] Z. G. Wang,[1,a] Z. H. Wang,[46,a] Z. Y. Wang,[1] Z. Y. Wang,[1] T. Weber,[22] D. H. Wei,[11] J. B. Wei,[31] P. Weidenkaff,[22] S. P. Wen,[1] U. Wiedner,[4] M. Wolke,[50] L. H. Wu,[1] L. J. Wu,[1] Z. Wu,[1,a] L. Xia,[46,a] L. G. Xia,[39] Y. Xia,[18] D. Xiao,[1] H. Xiao,[47] Z. J. Xiao,[28] Y. G. Xie,[1,a] Q. L. Xiu,[1,a] G. F. Xu,[1] J. J. Xu,[1] L. Xu,[1] Q. J. Xu,[13] X. P. Xu,[37] L. Yan,[49a,49c] W. B. Yan,[46,a] W. C. Yan,[46,a] Y. H. Yan,[18] H. J. Yang,[34] H. X. Yang,[1] L. Yang,[51] Y. Yang,[6] Y. X. Yang,[11] M. Ye,[1,a] M. H. Ye,[7] J. H. Yin,[1] B. X. Yu,[1,a] C. X. Yu,[30] J. S. Yu,[26] C. Z. Yuan,[1] W. L. Yuan,[29] Y. Yuan,[1] A. Yuncu,[40b,c] A. A. Zafar,[48] A. Zallo,[20a] Y. Zeng,[18] Z. Zeng,[46,a] B. X. Zhang,[1] B. Y. Zhang,[1,a] C. Zhang,[29] C. C. Zhang,[1] D. H. Zhang,[1] H. H. Zhang,[38] H. Y. Zhang,[1,a] J. Zhang,[1] J. J. Zhang,[1] J. L. Zhang,[1] J. Q. Zhang,[1] J. W. Zhang,[1,a] J. Y. Zhang,[1] J. Z. Zhang,[1] K. Zhang,[1] L. Zhang,[1] X. Y. Zhang,[33] Y. Zhang,[1] Y. N. Zhang,[41] Y. H. Zhang,[1,a] Y. T. Zhang,[46,a] Yu Zhang,[41] Z. H. Zhang,[6] Z. P. Zhang,[46] Z. Y. Zhang,[51] G. Zhao,[1] J. W. Zhao,[1,a] J. Y. Zhao,[1] J. Z. Zhao,[1,a] Lei Zhao,[46,a] Ling Zhao,[1] M. G. Zhao,[30] Q. Zhao,[1] Q. W. Zhao,[1] S. J. Zhao,[53] T. C. Zhao,[1] Y. B. Zhao,[1,a] Z. G. Zhao,[46,a] A. Zhemchugov,[23,d] B. Zheng,[47] J. P. Zheng,[1,a] W. J. Zheng,[33] Y. H. Zheng,[41] B. Zhong,[28] L. Zhou,[1,a] X. Zhou,[51] X. K. Zhou,[46,a] X. R. Zhou,[46,a] X. Y. Zhou,[1] K. Zhu,[1] K. J. Zhu,[1,a] S. Zhu,[1] S. H. Zhu,[45] X. L. Zhu,[39] Y. C. Zhu,[46,a] Y. S. Zhu,[1] Z. A. Zhu,[1] J. Zhuang,[1,a] L. Zotti,[49a,49c] B. S. Zou,[1] and J. H. Zou[1]

(BESIII Collaboration)

[1]*Institute of High Energy Physics, Beijing 100049, People's Republic of China*
[2]*Beihang University, Beijing 100191, People's Republic of China*
[3]*Beijing Institute of Petrochemical Technology, Beijing 102617, People's Republic of China*

[4]*Bochum Ruhr-University, D-44780 Bochum, Germany*
[5]*Carnegie Mellon University, Pittsburgh, Pennsylvania 15213, USA*
[6]*Central China Normal University, Wuhan 430079, People's Republic of China*
[7]*China Center of Advanced Science and Technology, Beijing 100190, People's Republic of China*
[8]*COMSATS Institute of Information Technology, Lahore, Defence Road, Off Raiwind Road, 54000 Lahore, Pakistan*
[9]*G.I. Budker Institute of Nuclear Physics SB RAS (BINP), Novosibirsk 630090, Russia*
[10]*GSI Helmholtzcentre for Heavy Ion Research GmbH, D-64291 Darmstadt, Germany*
[11]*Guangxi Normal University, Guilin 541004, People's Republic of China*
[12]*GuangXi University, Nanning 530004, People's Republic of China*
[13]*Hangzhou Normal University, Hangzhou 310036, People's Republic of China*
[14]*Helmholtz Institute Mainz, Johann-Joachim-Becher-Weg 45, D-55099 Mainz, Germany*
[15]*Henan Normal University, Xinxiang 453007, People's Republic of China*
[16]*Henan University of Science and Technology, Luoyang 471003, People's Republic of China*
[17]*Huangshan College, Huangshan 245000, People's Republic of China*
[18]*Hunan University, Changsha 410082, People's Republic of China*
[19]*Indiana University, Bloomington, Indiana 47405, USA*
[20a]*INFN Laboratori Nazionali di Frascati, I-00044 Frascati, Italy*
[20b]*INFN and University of Perugia, I-06100 Perugia, Italy*
[21a]*INFN Sezione di Ferrara, I-44122 Ferrara, Italy*
[21b]*University of Ferrara, I-44122 Ferrara, Italy*
[22]*Johannes Gutenberg University of Mainz, Johann-Joachim-Becher-Weg 45, D-55099 Mainz, Germany*
[23]*Joint Institute for Nuclear Research, 141980 Dubna, Moscow region, Russia*
[24]*Justus Liebig University Giessen, II. Physikalisches Institut, Heinrich-Buff-Ring 16, D-35392 Giessen, Germany*
[25]*KVI-CART, University of Groningen, NL-9747 AA Groningen, Netherlands*
[26]*Lanzhou University, Lanzhou 730000, People's Republic of China*
[27]*Liaoning University, Shenyang 110036, People's Republic of China*
[28]*Nanjing Normal University, Nanjing 210023, People's Republic of China*
[29]*Nanjing University, Nanjing 210093, People's Republic of China*
[30]*Nankai University, Tianjin 300071, People's Republic of China*
[31]*Peking University, Beijing 100871, People's Republic of China*
[32]*Seoul National University, Seoul, 151-747 Korea*
[33]*Shandong University, Jinan 250100, People's Republic of China*
[34]*Shanghai Jiao Tong University, Shanghai 200240, People's Republic of China*
[35]*Shanxi University, Taiyuan 030006, People's Republic of China*
[36]*Sichuan University, Chengdu 610064, People's Republic of China*
[37]*Soochow University, Suzhou 215006, People's Republic of China*
[38]*Sun Yat-Sen University, Guangzhou 510275, People's Republic of China*
[39]*Tsinghua University, Beijing 100084, People's Republic of China*
[40a]*Istanbul Aydin University, 34295 Sefakoy, Istanbul, Turkey*
[40b]*Dogus University, 34722 Istanbul, Turkey*
[40c]*Uludag University, 16059 Bursa, Turkey*
[40d]*Near East University, Nicosia, North Cyprus, 10, Mersin 99138, Turkey*
[41]*University of Chinese Academy of Sciences, Beijing 100049, People's Republic of China*
[42]*University of Hawaii, Honolulu, Hawaii 96822, USA*
[43]*University of Minnesota, Minneapolis, Minnesota 55455, USA*
[44]*University of Rochester, Rochester, New York 14627, USA*
[45]*University of Science and Technology Liaoning, Anshan 114051, People's Republic of China*
[46]*University of Science and Technology of China, Hefei 230026, People's Republic of China*
[47]*University of South China, Hengyang 421001, People's Republic of China*
[48]*University of the Punjab, Lahore 54590, Pakistan*
[49a]*University of Turin, I-10125 Turin, Italy*
[49b]*University of Eastern Piedmont, I-15121 Alessandria, Italy*
[49c]*INFN, I-10125 Turin, Italy*
[50]*Uppsala University, Box 516, SE-75120 Uppsala, Sweden*

[51]Wuhan University, Wuhan 430072, People's Republic of China
[52]Zhejiang University, Hangzhou 310027, People's Republic of China
[53]Zhengzhou University, Zhengzhou 450001, People's Republic of China
(Received 26 December 2015; published 4 August 2016)

We present an analysis of the decay $D^+ \to K^-\pi^+e^+\nu_e$ based on data collected by the BESIII experiment at the $\psi(3770)$ resonance. Using a nearly background-free sample of 18262 events, we measure the branching fraction $\mathcal{B}(D^+ \to K^-\pi^+e^+\nu_e) = (3.77 \pm 0.03 \pm 0.08)\%$. For $0.8 < m_{K\pi} < 1.0$ GeV/c^2, the partial branching fraction is $\mathcal{B}(D^+ \to K^-\pi^+e^+\nu_e)_{[0.8,1.0]} = (3.39 \pm 0.03 \pm 0.08)\%$. A partial wave analysis shows that the dominant $\bar{K}^*(892)^0$ component is accompanied by an S-wave contribution accounting for $(6.05 \pm 0.22 \pm 0.18)\%$ of the total rate and that other components are negligible. The parameters of the $\bar{K}^*(892)^0$ resonance and of the form factors based on the spectroscopic pole dominance predictions are also measured. We also present a measurement of the $\bar{K}^*(892)^0$ helicity basis form factors in a model-independent way.

DOI: 10.1103/PhysRevD.94.032001

I. INTRODUCTION

The semileptonic decay $D^+ \to K^-\pi^+e^+\nu_e$, named D_{e4} decay, has received particular attention due to the relative simplicity of its theoretical description and the large branching fraction. The matrix element of D_{e4} decay can be factorized as the product of the leptonic and hadronic currents. This makes it a natural place to study the $K\pi$ system in the absence of interactions with other hadrons and to determine the hadronic transition form factors. In this paper, the analysis is done mainly for two purposes:

(i) Measure the different $K\pi$ resonant and nonresonant amplitudes that contribute to this decay, including S-wave and radially excited P-wave and D-wave components. Accurate measurements of these contributions can provide helpful information for amplitude analyses of D-meson and B-meson decays.
(ii) Measure the q^2-dependent transition form factors in the D_{e4} decay, where q^2 is the invariant mass squared of the $e\nu_e$ system. This can be compared with hadronic model expectations and lattice QCD computations [1].

The decay $D^+ \to K^-\pi^+e^+\nu_e$ proceeds dominantly through the $\bar{K}^*(892)^0$ vector resonance. High statistics in this decay allow accurate measurements of the $\bar{K}^*(892)^0$ resonance parameters. Besides this dominant process, both FOCUS and *BABAR* have observed an S-wave contribution with a fraction of about 6% in this D_{e4} decay [2,3]. In *BABAR*'s parametrization, the $K\pi$ S wave with the isospin of $I = 1/2$ was composed of a nonresonant background term and the $\bar{K}_0^*(1430)^0$ [3]. The S-wave modulus was parametrized as a polynomial dependence on the $K\pi$ mass for the nonresonant component and a Breit-Wigner shape for the $\bar{K}_0^*(1430)^0$. The phase was parametrized based on measurements of the LASS scattering experiment [4]. It was described as a sum of the background term $\delta_{\rm BG}^{1/2}$ and the $\bar{K}_0^*(1430)^0$ term $\delta_{\bar{K}_0^*(1430)}^0$, where the mass dependence of $\delta_{\rm BG}^{1/2}$ was described by means of an effective range parametrization. *BABAR* used it to fit the data over a $K\pi$ invariant mass $m_{K\pi}$ range up to 1.6 GeV/c^2, showing that this parametrization could describe the data well. In addition, they did a model-independent measurement of the phase variation with $m_{K\pi}$, which agreed well with the fit result based on the LASS parametrization. In this paper, we use *BABAR*'s parametrization to describe the S wave and perform a model-independent measurement of its phase as well.

Another goal of this analysis is to describe the $D^+ \to K^-\pi^+e^+\nu_e$ decay in terms of helicity basis form factors that give the q^2-dependent amplitudes of the $K\pi$ system in any of its possible angular momentum states [5]. Traditionally, they are written as linear combinations of vector and axial-vector form factors which are assumed to depend on q^2 according to the spectroscopic pole dominance (SPD) model [5,6]. In this analysis, we present two ways to measure them. One way is to use the SPD model to describe the form factors in the partial wave analysis (PWA) framework. Another way is to perform a nonparametric

[a]Also at State Key Laboratory of Particle Detection and Electronics, Beijing 100049, Hefei 230026, People's Republic of China.
[b]Also at Ankara University, 06100 Tandogan, Ankara, Turkey.
[c]Also at Bogazici University, 34342 Istanbul, Turkey.
[d]Also at the Moscow Institute of Physics and Technology, Moscow 141700, Russia.
[e]Also at the Functional Electronics Laboratory, Tomsk State University, Tomsk, 634050, Russia.
[f]Also at the Novosibirsk State University, Novosibirsk, 630090, Russia.
[g]Also at the NRC "Kurchatov Institute," PNPI, 188300, Gatchina, Russia.
[h]Also at University of Texas at Dallas, Richardson, TX 75083, USA.
[i]Also at Istanbul Arel University, 34295 Istanbul, Turkey.

measurement of the q^2 dependence of the helicity basis form factors using a weighting technique, free from the SPD assumptions. This study will provide a better understanding of the semileptonic decay dynamics.

II. EXPERIMENTAL AND ANALYSIS DETAILS

The analysis is based on the data sample of 2.93 fb^{-1} [7,8] collected in e^+e^- annihilations at the $\psi(3770)$ peak, which has been accumulated with the BESIII detector operated at the double-ring Beijing Electron-Positron Collider II.

The BESIII detector [9] is designed approximately cylindrically symmetric around the interaction point, covering 93% of the solid angle. Starting from its innermost component, the BESIII detector consists of a 43-layer main drift chamber (MDC), a time-of-flight (TOF) system with two layers in the barrel region and one layer for each end cap, and a 6240-cell CsI(Tl) crystal electromagnetic calorimeter (EMC) with both barrel and end cap sections. The barrel components reside within a superconducting solenoidal magnet providing a 1.0 T magnetic field aligned with the beam axis. Finally, a muon chamber (MUC) consisting of nine layers of resistive plate chambers is incorporated within the return yoke of the magnet. In this analysis, the MUC information is not used. The momentum resolution for charged tracks in the MDC is 0.5% for transverse momenta of 1 GeV/c. The MDC also provides specific ionization ($\mathrm{d}E/\mathrm{d}x$) measurements for charged particles, with a resolution better than 6% for electrons from Bhabha scattering. The energy resolution for showers in the EMC is 2.5% for 1 GeV photons. The time resolution of the TOF is 80 ps in the barrel and 110 ps in the end caps.

A GEANT4-based detector simulation [10] is used to study the detector performance. The production of the $\psi(3770)$ resonance is simulated by the generator KKMC [11], which takes the beam energy spread and the initial-state radiation (ISR) into account. The decays of Monte Carlo (MC) events are generated with EvtGen [12]. The final-state radiation of charged particles is considered with the PHOTOS package [13]. Two types of MC samples are involved in this analysis: "generic MC" and "signal MC." Generic MC consists of $D\bar{D}$ and non-$D\bar{D}$ decays of $\psi(3770)$, ISR production of low-mass ψ states, and QED and $q\bar{q}$ continuum processes. The effective luminosities of the above MC samples correspond to five to ten times those of the experimental data. All the known decay modes are generated with the branching fractions taken from the Particle Data Group (PDG) [14], while the remaining unknown processes are simulated with LundCharm [15]. Signal MC is produced to simulate exclusive $\psi(3770) \to D^+D^-$ decays, where D^+ decays to the semileptonic signals uniformly (named "PHSP signal MC") or with the decay intensity distribution determined by PWA (named "PWA signal MC"), while D^- decays inclusively as in generic MC.

We use the technique of tagged D-meson decays [16]. At 3.773 GeV annihilation energy, D mesons are produced in pairs. If a decay of one D meson ("tagged decay") has been fully reconstructed in an event, then the existence of another $\bar{D}$ decay ("signal decay") in the same event is guaranteed. The tagged decays are reconstructed in the channels with larger branching fractions and lower background levels. Six decay channels are considered: $D^- \to K^+\pi^-\pi^-$, $D^- \to K^+\pi^-\pi^-\pi^0$, $D^- \to K^0_S\pi^-$, $D^- \to K^0_S\pi^-\pi^0$, $D^- \to K^0_S\pi^-\pi^-\pi^+$, and $D^- \to K^+K^-\pi^-$. The event selection consists of several stages: selection and identification of particles (tracks and electromagnetic showers), selection of the tagged decays, and selection of the signal decays $D^+ \to K^-\pi^+e^+\nu_e$. Throughout this paper, unless explicitly stated otherwise, the charge conjugate is also implied when a decay mode of a specific charge is stated.

Good tracks of charged particles are selected by the requirement that the track origin is close to the interaction point (within 10 cm along the beam axis and within 1 cm in the perpendicular plane) and that the polar angle θ between the track and the beam direction is within the good detector acceptance, $|\cos\theta| < 0.93$. The photons used for the neutral pion reconstruction are selected as electromagnetic showers with a minimum energy of 25 MeV in the barrel region ($|\cos\theta| < 0.8$) or 50 MeV in the end caps ($0.86 < |\cos\theta| < 0.92$). The shower timing measured by the calorimeter has to be within 700 ns after the beam collision.

Charged particle identification (PID) for pions and kaons is based on the combined measurements of the $\mathrm{d}E/\mathrm{d}x$ and TOF. Hypotheses for the track to be pion or kaon are considered. Each track is characterized by $P(\pi)$ and $P(K)$, which are the likelihoods for the pion and kaon hypotheses. The pion candidates are identified with the requirement $P(\pi) > P(K)$, and the kaon candidates are required to have $P(K) > P(\pi)$.

The electron identification includes the measurements of the energy deposition in the EMC in addition to the $\mathrm{d}E/\mathrm{d}x$ and TOF information. The measured values are used to calculate the likelihoods P_2 for different particle hypotheses. The electron candidates have to satisfy the following criteria: $P_2(e)/((P_2(K)+P_2(\pi)+P_2(e)) > 0.8$, $P_2(e) > 0.001$. Additionally, the EMC energy of the electron candidate has to be more than 80% of the track momentum measured in the MDC.

Neutral pions are reconstructed from pairs of good photons with an invariant mass in the range $115 < M_{\gamma\gamma} < 150\ \text{MeV}/c^2$ and with a χ^2 value for the one-constraint (1-C) mass constrained kinematic fit of $\pi^0 \to \gamma\gamma$ less than 200. Candidates with both photons from the EMC end cap regions are rejected.

Neutral K^0_S candidates are reconstructed with pairs of oppositely charged tracks which are constrained to have a common vertex. The tracks from the K^0_S decay are not

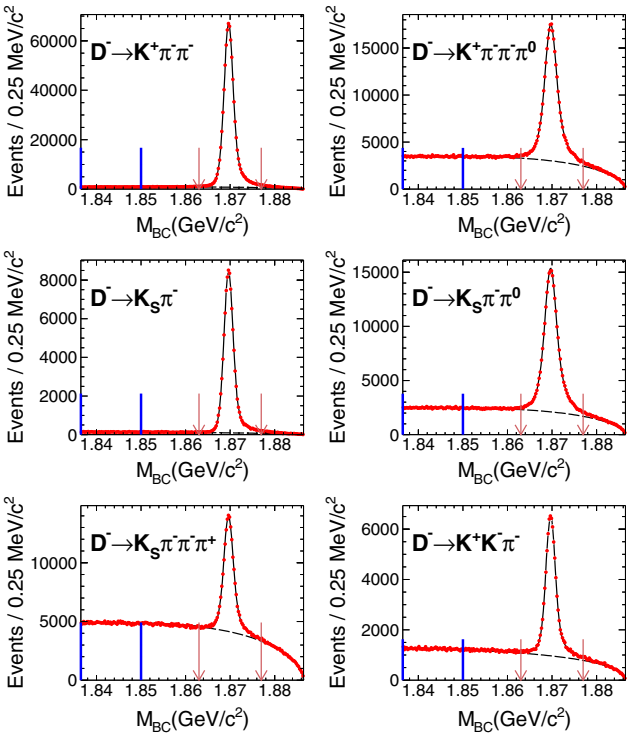

FIG. 1. Fits to the $M_{\rm BC}$ distributions for different tagged decay channels. The dots with error bars represent data, and the solid curves show the fits, which are the sum of signals and background events. The background components are shown by the dashed lines. The areas between the arrows represent the signal regions, while those between the vertical solid lines show the sidebands.

required to satisfy the good track selection or PID criteria. Assuming the two tracks to be pions, we require them to have an invariant mass in the range $487 < M_{\pi^+\pi^-} < 511$ MeV$/c^2$. The closest approach of the track should be within 20 cm from the interaction point along the beam direction, and the polar angle has to satisfy $|\cos\theta| < 0.93$.

Appropriate combinations of the charged tracks and photons are formed for the six tagged D^- decay channels. Two variables are calculated for each possible track combination: $M_{\rm BC} = \sqrt{E^2_{\rm beam} - |\vec{p}_D|^2}$, $\Delta E = E_D - E_{\rm beam}$, where E_D and $\vec{p}_D$ are the reconstructed energy and momentum of the D^- candidate, and $E_{\rm beam}$ is the beam energy. ΔE is required to be consistent with zero within approximately twice the experimental resolution, while $M_{\rm BC}$ should be within the signal region $1.863 < M_{\rm BC} < 1.877$ GeV$/c^2$. In each event, we accept at most one candidate per tag mode per charge; in the case of multiple candidates, the one with the smallest ΔE is chosen.

The tagged decay yields are determined separately for the six tag channels. The yields are obtained by fitting the signal and background contributions to the $M_{\rm BC}$ distribution (Fig. 1) of the events passing the ΔE cuts. The signal shape is modeled by the reconstructed MC distribution, while the background shape is described by the ARGUS function [17]. The yields are determined by subtracting the numbers of background events from the total numbers of events in the $M_{\rm BC}$ signal region. The yields of the six tags $N_{\rm tag}$, together with the tag efficiencies $\epsilon_{\rm tag}$ estimated by generic MC, are listed in Table I.

The signal decay $D^+ \to K^-\pi^+e^+\nu_e$ is reconstructed from the tracks remaining after the selection of the D^- tag. We require that there are exactly three tracks on the signal side satisfying the good track selection criteria, and they must be identified as K^-, π^+, and e^+.

The energy $E_{\rm miss}$ and momentum $\vec{p}_{\rm miss}$ of the missing neutrino are reconstructed using energy and momentum conservation. Background events with an undetected massive particle are suppressed by the requirement $|U_{\rm miss}| < 0.04$ GeV, where $U_{\rm miss} = E_{\rm miss} - |\vec{p}_{\rm miss}|$. The background from neutrinoless decays is suppressed by the selection criterion $E_{\rm miss} > 0.04$ GeV.

The background from the events containing neutral pions is suppressed by the requirement that no unassociated EMC shower has an energy deposition above 0.25 GeV. Only the clusters separated by more than 15° from the closest charged tracks are considered.

Finally, in order to reject cross-feed from the $e^+e^- \to D^0\bar{D}^0$ events, an additional selection is applied to the events where the tagged decay is reconstructed in the channels $D^- \to K^0_S\pi^-\pi^-\pi^+$, $D^- \to K^0_S\pi^-\pi^0$, and $D^- \to K^+\pi^-\pi^-\pi^0$. For such events, reconstruction of a purely hadronic decay of a neutral D^0 or $\bar{D}^0$ meson is attempted using the tracks from the entire event. The event is rejected if any D^0 candidate satisfies the tight selection criteria $1.860 < M_{\rm BC} < 1.875$ GeV$/c^2$ and $|\Delta E| < 0.01$ GeV.

TABLE I. Summary of event selection for different tag modes, where the errors are statistical.

Tag	$N_{\rm tag}$	$\epsilon_{\rm tag}$ (%)	$\epsilon_{\rm tag,sig}$ in full $m_{K\pi}$ range (%)	$\epsilon_{\rm tag,sig}$ in K^*-dominated region (%)
$K^+\pi^-\pi^-$	776648 ± 915	50.62 ± 0.02	16.46 ± 0.02	16.30 ± 0.02
$K^+\pi^-\pi^-\pi^0$	234979 ± 678	25.23 ± 0.02	7.71 ± 0.02	7.62 ± 0.02
$K^0_S\pi^-$	95498 ± 320	53.91 ± 0.06	17.55 ± 0.07	17.34 ± 0.07
$K^0_S\pi^-\pi^0$	215619 ± 610	29.24 ± 0.03	9.06 ± 0.02	8.95 ± 0.02
$K^0_S\pi^-\pi^-\pi^+$	120491 ± 648	37.33 ± 0.06	11.55 ± 0.04	11.00 ± 0.04
$K^-K^+\pi^-$	69909 ± 374	40.78 ± 0.07	13.18 ± 0.06	13.04 ± 0.06

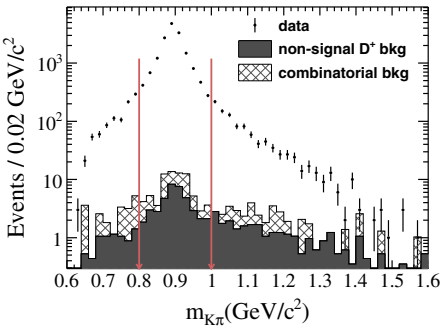

FIG. 2. $m_{K\pi}$ distribution of the selected candidates. The range between the arrows corresponds to the K^*-dominated region. The dots with error bars represent data, the shadowed histogram shows the nonsignal D^+ background estimated from MC simulation, and the hatched area shows the combinatorial background estimated from the $M_{\rm BC}$ sideband of data.

In total, 18262 candidates are selected (denoted as $N_{\rm obs}$). The $m_{K\pi}$ distribution of these candidates is illustrated in Fig. 2 in the full $m_{K\pi}$ range $0.6 < m_{K\pi} < 1.6$ GeV/c^2. In the K^*-dominated region $0.8 < m_{K\pi} < 1.0$ GeV/c^2 (corresponding to the area between the arrows), 16181 candidates are located.

MC simulation shows that the background level is about 0.8% over the full $m_{K\pi}$ range and around 0.5% in the K^*-dominated region. The backgrounds can be divided into two categories. One category arises from nonsignal D^+ decays, including $D^+ \to K^-\pi^+\pi^+\pi^0$, $D^+ \to K^-\pi^+\pi^+$, and $D^+ \to K^-\pi^+\mu^+\nu_\mu$, among which the last one is the largest contribution, arising when μ^+ is misidentified as e^+. For the nonsignal D^+ background, the accompanying D^- meson peaks in the $M_{\rm BC}$ distribution in the same way as when D^+ decays to signals. The number of this background is estimated using MC simulation, 76 ± 3 over the full $m_{K\pi}$ range and 40 ± 2 in the K^*-dominated region (the errors are statistical only). The other category is combinatorial background, mainly due to $e^+e^- \to D^0\bar{D}^0$ events and the $e^+e^- \to q\bar{q}$ continuum. This background has a continuum $M_{\rm BC}$ spectrum and can be estimated from data using the events located in the sideband (see Fig. 1). The scaled contribution from this background is 69 ± 7 and 33 ± 5 over the full $m_{K\pi}$ range and in the K^*-dominated region, respectively. The backgrounds from both categories are illustrated in Fig. 2, and the total number (denoted as $N_{\rm bkg}$) can be obtained by summing them up.

III. DETERMINATION OF THE BRANCHING FRACTION

The branching fraction of the decay $D^+ \to K^-\pi^+e^+\nu_e$ is calculated using

$$\mathcal{B}_{\rm sig} = \frac{N_{\rm obs} - N_{\rm bkg}}{\sum_\alpha N^\alpha_{\rm tag}\epsilon^\alpha_{{\rm tag},sig}/\epsilon^\alpha_{\rm tag}}, \quad (1)$$

where $N_{\rm obs}$ and $N_{\rm bkg}$ are the numbers of the observed and the background events (see Sec. II). For the tag mode α, $N^\alpha_{\rm tag}$ is the number of the tagged D^- mesons, $\epsilon^\alpha_{\rm tag}$ is the reconstruction efficiency, and $\epsilon^\alpha_{\rm tag,sig}$ represents the combined efficiency to reconstruct both D^+ and D^-.

The selection efficiency $\epsilon_{\rm tag,sig}$ depends significantly on the relative contribution of different $(K\pi)$ states. Therefore, we exploit two ways to calculate the branching fraction. One way is to use the PWA method to estimate precisely the contributions from different processes in the $D^+ \to K^-\pi^+e^+\nu_e$ final state. $\epsilon_{\rm tag,sig}$ is determined by signal MC which is based on the PWA results. Another way is to determine the branching fraction in the K^*-dominated region. This region is dominated by the $\bar{K}^*(892)^0$ resonance, and the determination of the branching fraction is nearly independent of the model describing the composition of the decay.

The PWA procedure will be described in detail in Sec. IV. The selection efficiencies $\epsilon_{\rm tag,sig}$ for both the methods are summarized in Table I. The resulting branching fractions are obtained over the full $m_{K\pi}$ range and in the K^*-dominated region as

$$\mathcal{B}(D^+ \to K^-\pi^+e^+\nu_e) = (3.77 \pm 0.03 \pm 0.08)\%, \quad (2)$$

$$\mathcal{B}(D^+ \to K^-\pi^+e^+\nu_e)_{[0.8,1.0]} = (3.39 \pm 0.03 \pm 0.08)\%, \quad (3)$$

where the first errors are statistical and the second are systematic.

The largest contributions to the systematic uncertainties for the branching fraction originate from the MC determination of the efficiencies of track reconstruction (1.73%) and particle identification (0.95%). They are estimated using clean samples of pions, kaons, and electrons.

The uncertainties due to the selection criteria are estimated by comparing the corresponding selection efficiencies between data and MC using clean control samples. The uncertainty due to the $U_{\rm miss}$ requirement (0.76%) is estimated using fully reconstructed $D^+ \to K^-\pi^+\pi^+$, $D^- \to K^+\pi^-\pi^-\pi^0$ decays by treating one photon as a missing particle. The uncertainty due to the selection on the electron E/p ratio (0.36%) is obtained using electrons from radiative Bhabha scattering. To obtain the uncertainty due to the shower isolation requirement (0.26%), fully reconstructed $D^+ \to K^-\pi^+\pi^+$, $D^- \to K^+\pi^-\pi^-$ decays are used.

We vary the $M_{\rm BC}$ fit range to estimate the associated uncertainty (0.32%). We also consider uncertainties due to imperfections of the PWA model (0.23%). This is estimated by varying parameters in the probability density function (PDF) [the detail of which will be described in Eq. (22)] by 1σ and considering additional resonances. To estimate the uncertainty due to the background fraction (0.16%), we change the branching fractions by 1σ according to PDG for

the nonsignal D^+ background and vary the normalization by 1σ for the combinatorial background. As for the uncertainty due to the shape of the background distribution (0.12%), only the uncertainty from the $D^+ \to K^-\pi^+\pi^+\pi^0$ background is non-negligible, which is estimated by comparing the difference between two extreme cases: phase space process and $D^+ \to \bar{K}^*(892)^0\rho^+$.

The total systematic uncertainties are calculated by adding the above uncertainties in quadrature, resulting in 2.21% for both the branching fraction over the full $m_{K\pi}$ range and in the K^*-dominated region.

IV. PWA OF $D^+ \to K^-\pi^+e^+\nu_e$ DECAY

The four-body decay $D^+ \to K^-\pi^+e^+\nu_e$ can be uniquely described by the five kinematic variables [18]: $K\pi$ mass square (m^2), $e\nu_e$ mass square (q^2), the angle between the π and the D direction in the $K\pi$ rest frame (θ_K), the angle between the ν_e and the D direction in the $e\nu_e$ rest frame (θ_e), and the angle between the two decay planes (χ). The angular variables are illustrated in Fig. 3. The sign of χ should be changed when analyzing D^- in order to maintain CP conservation.

Neglecting the mass of e^+, the differential decay width can be expressed as

$$\begin{aligned} d^5\Gamma &= \frac{G_F^2|V_{cs}|^2}{(4\pi)^6 m_D^3} X\beta\mathcal{I}(m^2, q^2, \theta_K, \theta_e, \chi) \\ &\quad \times dm^2 dq^2 d\cos(\theta_K) d\cos(\theta_e) d\chi, \\ X &= p_{K\pi} m_D, \qquad \beta = 2p^*/m, \end{aligned} \tag{4}$$

where G_F is the Fermi constant, V_{cs} is the $c \to s$ element of the Cabibbo-Kobayashi-Maskawa matrix, $p_{K\pi}$ is the momentum of the $K\pi$ system in the D rest frame, and p^* is the momentum of the K in the $K\pi$ rest frame. The dependence of the decay intensity $\mathcal{I}$ on θ_e and χ is given by Ref. [19],

$$\begin{aligned} \mathcal{I} &= \mathcal{I}_1 + \mathcal{I}_2\cos 2\theta_e + \mathcal{I}_3\sin^2\theta_e\cos 2\chi + \mathcal{I}_4\sin 2\theta_e\cos\chi \\ &\quad + \mathcal{I}_5\sin\theta_e\cos\chi + \mathcal{I}_6\cos\theta_e + \mathcal{I}_7\sin\theta_e\sin\chi \\ &\quad + \mathcal{I}_8\sin 2\theta_e\sin\chi + \mathcal{I}_9\sin^2\theta_e\sin 2\chi, \end{aligned} \tag{5}$$

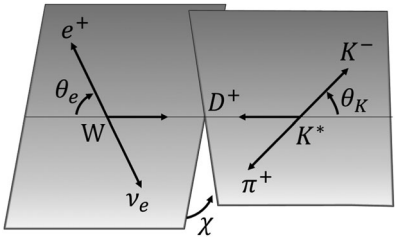

FIG. 3. Definition of the angular variables.

where $\mathcal{I}_{1,\ldots,9}$ depend on m^2, q^2, and θ_K. These quantities can be expressed in terms of the three form factors $\mathcal{F}_{1,2,3}$:

$$\begin{aligned} \mathcal{I}_1 &= \frac{1}{4}\left\{|\mathcal{F}_1|^2 + \frac{3}{2}\sin^2\theta_K(|\mathcal{F}_2|^2 + |\mathcal{F}_3|^2)\right\}, \\ \mathcal{I}_2 &= -\frac{1}{4}\left\{|\mathcal{F}_1|^2 - \frac{1}{2}\sin^2\theta_K(|\mathcal{F}_2|^2 + |\mathcal{F}_3|^2)\right\}, \\ \mathcal{I}_3 &= -\frac{1}{4}\{|\mathcal{F}_2|^2 - |\mathcal{F}_3|^2\}\sin^2\theta_K, \\ \mathcal{I}_4 &= \frac{1}{2}\mathrm{Re}(\mathcal{F}_1^*\mathcal{F}_2)\sin\theta_K, \\ \mathcal{I}_5 &= \mathrm{Re}(\mathcal{F}_1^*\mathcal{F}_3)\sin\theta_K, \\ \mathcal{I}_6 &= \mathrm{Re}(\mathcal{F}_2^*\mathcal{F}_3)\sin^2\theta_K, \\ \mathcal{I}_7 &= \mathrm{Im}(\mathcal{F}_1\mathcal{F}_2^*)\sin\theta_K, \\ \mathcal{I}_8 &= \frac{1}{2}\mathrm{Im}(\mathcal{F}_1\mathcal{F}_3^*)\sin\theta_K, \\ \mathcal{I}_9 &= -\frac{1}{2}\mathrm{Im}(\mathcal{F}_2\mathcal{F}_3^*)\sin^2\theta_K. \end{aligned} \tag{6}$$

Then, one can expand $\mathcal{F}_{i=1,2,3}$ into partial waves including the S wave ($\mathcal{F}_{10}$), P wave ($\mathcal{F}_{i1}$), and D wave ($\mathcal{F}_{i2}$):

$$\begin{aligned} \mathcal{F}_1 &= \mathcal{F}_{10} + \mathcal{F}_{11}\cos\theta_K + \mathcal{F}_{12}\frac{3\cos^2\theta_K - 1}{2}, \\ \mathcal{F}_2 &= \frac{1}{\sqrt{2}}\mathcal{F}_{21} + \sqrt{\frac{3}{2}}\mathcal{F}_{22}\cos\theta_K, \\ \mathcal{F}_3 &= \frac{1}{\sqrt{2}}\mathcal{F}_{31} + \sqrt{\frac{3}{2}}\mathcal{F}_{32}\cos\theta_K. \end{aligned} \tag{7}$$

Here, the parametrizations of $\mathcal{F}_{ij}$ are taken from the *BABAR* Collaboration [3]. Contributions with higher angular momenta are neglected.

The P-wave related form factors $\mathcal{F}_{i1}$ are parametrized by the helicity basis form factors $H_{0,\pm}$:

$$\begin{aligned} \mathcal{F}_{11} &= 2\sqrt{2}\alpha q H_0 \times \mathcal{A}(m), \\ \mathcal{F}_{21} &= 2\alpha q(H_+ + H_-) \times \mathcal{A}(m), \\ \mathcal{F}_{31} &= 2\alpha q(H_+ - H_-) \times \mathcal{A}(m). \end{aligned} \tag{8}$$

Here, $\mathcal{A}(m)$ denotes the amplitude characterizing the shape of the resonances, which has a Breit-Wigner form defined in Eq. (11). α is a constant factor given in Eq. (15), which depends on the definition of $\mathcal{A}(m)$. The factorization in Eq. (8) and in the following Eqs. (16) and (21) is based on the assumption that the q^2 dependence of the resonance amplitude is weak for the narrow Breit-Wigner structure. The helicity basis form factors can be related to one vector $V(q^2)$ and two axial-vector $A_{1,2}(q^2)$ form factors:

$$H_0(q^2,m^2)=\frac{1}{2mq}\left[(m_D^2-m^2-q^2)(m_D+m)A_1(q^2)-4\frac{m_D^2p_{K\pi}^2}{m_D+m}A_2(q^2)\right],$$
$$H_\pm(q^2,m^2)=\left[(m_D+m)A_1(q^2)\mp\frac{2m_Dp_{K\pi}}{(m_D+m)}V(q^2)\right]. \quad (9)$$

The q^2 dependence is expected to be determined by the singularities nearest to the q^2 physical region [0, $q^2_{\rm max}$] ($q^2_{\rm max}\sim 1.25\ {\rm GeV}^2/c^4$), which are assumed to be poles corresponding to the lowest vector (D_S^*) and axial-vector (D_{S1}) states for the vector and axial-vector form factors, respectively. We use the SPD model to describe the q^2 dependence,

$$V(q^2)=\frac{V(0)}{1-q^2/m_V^2},$$
$$A_1(q^2)=\frac{A_1(0)}{1-q^2/m_A^2},$$
$$A_2(q^2)=\frac{A_2(0)}{1-q^2/m_A^2}, \quad (10)$$

where m_V and m_A are expected to be close to $m_{D_S^*}\backsimeq 2.1\ {\rm GeV}/c^2$ and $m_{D_{S1}}\backsimeq 2.5\ {\rm GeV}/c^2$, respectively. In this analysis, the values of m_V, m_A, and the ratios of the form factors taken at $q^2=0$, $r_V=V(0)/A_1(0)$, and $r_2=A_2(0)/A_1(0)$, are determined by the PWA fit. The value of $A_1(0)$ is determined by measuring the branching fraction of $D^+\to\bar{K}^*(892)^0e^+\nu_e$.

For the amplitude of the resonance $\mathcal{A}(m)$, we use a Breit-Wigner shape with a mass-dependent width,

$$\mathcal{A}(m)=\frac{m_0\Gamma_0F_J(m)}{m_0^2-m^2-im_0\Gamma(m)}, \quad (11)$$

where m_0 and Γ_0 are the pole mass and total width of the resonance, respectively. This parametrization is applicable to resonances of different angular momenta denoted by J. In the case of the P wave, $J=1$. The mass-dependent width $\Gamma(m)$ is given by

$$\Gamma(m)=\Gamma_0\frac{p^*}{p_0^*}\frac{m_0}{m}F_J^2(m), \quad (12)$$

$$F_J=\left(\frac{p^*}{p_0^*}\right)^J\frac{B_J(p^*)}{B_J(p_0^*)}. \quad (13)$$

Here, p^* is the momentum of the K in the $K\pi$ rest frame, and p_0^* is its value determined at m_0, the pole mass of the resonance. B_J is the Blatt-Weisskopf damping factor given by the following expressions:

$$B_0(p)=1,$$
$$B_1(p)=1/\sqrt{1+r_{\rm BW}^2p^2},$$
$$B_2(p)=1/\sqrt{(r_{\rm BW}^2p^2-3)^2+9r_{\rm BW}^2p^2}. \quad (14)$$

The barrier factor $r_{\rm BW}$ as well as m_0 and Γ_0 for $\bar{K}^*(892)^0$ are free parameters in the PWA fit.

With the definition of the mass distribution given in Eq. (11), the factor α entering Eq. (8) is given by

$$\alpha=\sqrt{\frac{3\pi\mathcal{B}_{K^*}}{p_0^*\Gamma_0}}, \quad (15)$$

where $\mathcal{B}_{K^*}=\mathcal{B}(K^*\to K^-\pi^+)=2/3$.

The S-wave related form factor $\mathcal{F}_{10}$ is expressed as

$$\mathcal{F}_{10}=p_{K\pi}m_D\frac{1}{1-\frac{q^2}{m_A^2}}\mathcal{A}_S(m). \quad (16)$$

Here, the S-wave amplitude $\mathcal{A}_S(m)$ is considered as a combination of a nonresonant background and the $\bar{K}_0^*(1430)^0$. According to the Watson theorem [20], for the same isospin and angular momentum, the phase measured in $K\pi$ elastic scattering and in a decay channel are equal in the elastic regime. So, the formalism of the phase of the nonresonant background can be taken from the LASS scattering experiment [4]. The total S-wave phase $\delta_S(m)$ and the amplitude $\mathcal{A}_S(m)$ are parametrized in the same way as by the *BABAR* Collaboration [3],

$$\cot(\delta_{\rm BG}^{1/2})=\frac{1}{a_{\rm S,BG}^{1/2}p^*}+\frac{b_{\rm S,BG}^{1/2}p^*}{2}, \quad (17)$$

$$\cot(\delta_{\bar{K}_0^*(1430)^0})=\frac{m^2_{\bar{K}_0^*(1430)^0}-m^2}{m_{\bar{K}_0^*(1430)^0}\Gamma_{\bar{K}_0^*(1430)^0}(m)}, \quad (18)$$

$$\delta_S(m)=\delta_{\rm BG}^{1/2}+\delta_{\bar{K}_0^*(1430)^0}, \quad (19)$$

where the scattering length $a_{\rm S,BG}^{1/2}$ and the effective range $b_{\rm S,BG}^{1/2}$ are determined by the PWA fit. $m_{\bar{K}_0^*(1430)^0}$ is the pole mass of the $\bar{K}_0^*(1430)^0$. $\Gamma_{\bar{K}_0^*(1430)^0}(m)$ is its mass-dependent width, which can be calculated using Eq. (13) given the total width $\Gamma^0_{\bar{K}_0^*(1430)^0}$.

The amplitude $\mathcal{A}_S(m)$ is expressed as

$$\mathcal{A}_S(m) = r_S P(m) e^{i\delta_S(m)}, \quad m < m_{\bar{K}_0^*(1430)^0};$$
$$\mathcal{A}_S(m) = r_S P(m_{\bar{K}_0^*(1430)^0}) e^{i\delta_S(m)} \times \sqrt{\frac{(m_{\bar{K}_0^*(1430)^0}\Gamma^0_{\bar{K}_0^*(1430)^0})^2}{(m^2_{\bar{K}_0^*(1430)^0} - m^2)^2 + (m_{\bar{K}_0^*(1430)^0}\Gamma_{\bar{K}_0^*(1430)^0}(m))^2}}, \quad m > m_{\bar{K}_0^*(1430)^0}. \tag{20}$$

Here, $P(m) = 1 + x \cdot r_S^{(1)}$, and $x = \sqrt{(\frac{m}{m_K + m_\pi})^2 - 1}$. The dimensionless coefficient $r_S^{(1)}$ and the relative intensity r_S are determined by the PWA fit.

The D-wave related form factors F_{i2} are expressed similarly to those of the P wave:

$$\mathcal{F}_{12} = \frac{m_D p_{K\pi}}{3}\left[(m_D^2 - m^2 - q^2)(m_D + m)T_1(q^2) - \frac{m_D^2 p_{K\pi}^2}{m_D + m} T_2(q^2)\right]\mathcal{A}(m),$$
$$\mathcal{F}_{22} = \sqrt{\frac{2}{3}} m_D m q p_{K\pi}(m_D + m) T_1(q^2)\mathcal{A}(m),$$
$$\mathcal{F}_{32} = \sqrt{\frac{2}{3}} \frac{2m_D^2 m q p_{K\pi}^2}{m_D + m} T_V(q^2)\mathcal{A}(m). \tag{21}$$

For the D wave, we still assume that there are one vector $T_V(q^2)$ and two axial-vector $T_{1,2}(q^2)$ form factors, which behave according to the SPD model. Pole masses are assumed to be the same as those of the P wave, and the form factor ratios $r_{22} = T_2(0)/T_1(0)$ and $r_{2V} = T_V(0)/T_1(0)$ at $q^2 = 0$ are expected to be 1 [21]. The amplitude $\mathcal{A}(m)$ is described by the formula in Eq. (11) in the case of $J = 2$.

The PWA is performed using an unbinned maximum likelihood fit. The likelihood expression is

$$L = \prod_{i=1}^{N} \mathrm{PDF}(\xi_i, \eta) = \prod_{i=1}^{N} \frac{\omega(\xi_i, \eta)\epsilon(\xi_i)}{\int d\xi_i \omega(\xi_i, \eta)\epsilon(\xi_i)}, \tag{22}$$

where N denotes the number of the events in the PWA. PDF (ξ, η) is the probability density function with arguments ξ denoting the five kinematic variables characterizing the event and η denoting the fit parameters. $\omega(\xi, \eta)$ and $\epsilon(\xi)$ represent the decay intensity [i.e., $\mathcal{I}$ in Eq. (4)] and the acceptance for events of ξ.

Omitting the terms independent of the fit parameters, we obtain the negative log likelihood:

$$-\ln L = -\sum_{i=1}^{N} \ln \frac{\omega(\xi_i, \eta)}{\sigma(\eta)}. \tag{23}$$

The acceptance is taken into account in the term $\sigma(\eta)$, which is calculated using the PWA signal MC events that pass the event selection [22],

$$\sigma(\eta) = \int d\xi \omega(\xi, \eta)\epsilon(\xi) \propto \frac{1}{N_{\mathrm{selected}}} \sum_{k=1}^{N_{\mathrm{selected}}} \frac{\omega(\xi_k, \eta)}{\omega(\xi_k, \eta_0)}, \tag{24}$$

where η_0 denotes the set of the parameters used to produce the simulated events.

The effect of background in the fit is considered by subtracting its contribution in the likelihood calculation using Eq. (23),

$$-\ln L_{\mathrm{final}} = (-\ln L_{\mathrm{data}}) - (-\ln L_{\mathrm{bkg}}), \tag{25}$$

where L_{data} and L_{bkg} represent the likelihoods of the data sample and the background, respectively. $-\ln L_{\mathrm{final}}$ is minimized to determine the PWA solution. L_{bkg} is calculated using the nonsignal D^+ decays and the combinatorial background, as introduced in Sec. II.

The goodness of the fit is estimated using χ^2/n.d.f., where n.d.f. denotes the number of degrees of freedom. The χ^2 is calculated from the difference of the event distribution between data and MC predicted by the fit in the five-dimensional space of the kinematic variables m, q^2, $\cos\theta_K$, $\cos\theta_e$, and χ initially divided into 4, 3, 3, 3, and 3 bins. The bins are set with different sizes so that they contain an approximately equal number of signal events. Each five-dimensional bin is required to contain at least ten events; otherwise, it is combined with an adjacent bin. The χ^2 value is calculated as

$$\chi^2 = \sum_{i}^{N_{\mathrm{bin}}} \frac{(n_i^{\mathrm{data}} - n_i^{\mathrm{fit}})^2}{n_i^{\mathrm{fit}}}, \tag{26}$$

where N_{bin} is the number of the bins, n_i^{data} denotes the measured content of the ith bin, and n_i^{fit} denotes the expected ith bin content predicted by the fitted PDF. The n.d.f. is equal to the number of the bins (N_{bin}) minus the number of the fit parameters minus 1.

The structure of the $K\pi$ system is dominated by the $\bar{K}^*(892)^0$. As for other possible components, we determine their significances from the change of $-2\ln L$ in the PWA fits with and without the contribution of the component, taking into account the change of the n.d.f.. The contribution of the S wave [the $\bar{K}_0^*(1430)^0$ and the nonresonant part] is observed with a significance far larger than 10σ. The solution including the $\bar{K}^*(892)^0$ and the S wave, with the magnitude and phase of the $\bar{K}^*(892)^0$ component fixed at 1 and 0, is referred to here as the "nominal solution." The contribution from the $\bar{K}^*(1680)^0$ is ignored because it is suppressed by the small phase space available. We also assume the contribution from the κ to be negligible, as

follows from the FOCUS results [23]. Possible contributions from the $\bar{K}^*(1410)^0$ and $\bar{K}_2^*(1430)^0$ are searched.

The fraction of each component can be determined by the ratio of the decay intensity of the specific component and that of the total,

$$f_k = \frac{\int d\xi \omega_k(\xi,\eta)}{\int d\xi \omega(\xi,\eta)}, \tag{27}$$

where $\omega_k(\xi,\eta)$ and $\omega(\xi,\eta)$ denote the decay intensity of component k and the total, respectively.

The nominal solution of the PWA fit, together with the fractions of both components and the goodness of the fit, are listed in the second column of Table II. Comparisons of the projections over the five kinematic variables between data and the PWA solution are illustrated in Fig. 4.

Using the result of $\mathcal{B}(D^+ \to K^-\pi^+e^+\nu_e)$ from Eq. (2), the branching fractions of both components are calculated to be

$$\begin{aligned}\mathcal{B}(D^+ \to K^-\pi^+e^+\nu_e)_{S\text{-wave}} &= (0.228 \pm 0.008 \pm 0.008)\%,\\ \mathcal{B}(D^+ \to K^-\pi^+e^+\nu_e)_{\bar{K}^*(892)^0} &= (3.54 \pm 0.03 \pm 0.08)\%,\end{aligned} \tag{28}$$

where the first errors are statistical and the second systematic (described later in this section).

The nominal solution is based on the δ_S parametrization from Eq. (19). To test the applicability of this parametrization, the $m_{K\pi}$ spectrum is divided into 12 bins, and the PWA fit is performed with the phases δ_S in each bin as 12 additional fit parameters (within each bin, the phase is assumed to be constant). The measured invariant mass dependence of the phase is summarized in Table IV. All other parameters are consistent with those in the nominal fit. Figure 5 illustrates the comparison of the model-independent measurement with that based on the parametrization from Eq. (19).

Possible contributions from the $\bar{K}^*(1410)^0$ and $\bar{K}_2^*(1430)^0$ are studied by adding these resonances to the nominal solution with the complex coefficients $r_{\bar{K}^*(1410)^0}e^{i\delta_{\bar{K}^*(1410)^0}}$ and $r_{\bar{K}_2^*(1430)^0}e^{i\delta_{\bar{K}_2^*(1430)^0}}$. Because of the scarce population in the high $K\pi$ mass region, this analysis is not sensitive to the shapes of these resonances. Their masses and widths are therefore fixed at the values from the PDG. They are added to the nominal solution one by one. The effective range parameter $b_{\mathrm{S,BG}}^{1/2}$ is fixed at the result from the nominal solution. Based on the isobar model, time reversal symmetry requires the coupling constants for the $\bar{K}^*(1410)^0$ and $\bar{K}_2^*(1430)^0$ to be real, which means that the phases of the $\bar{K}^*(1410)^0$ and $\bar{K}_2^*(1430)^0$ are only allowed to be zero or π.

TABLE II. The PWA solutions with different combinations of S [the $\bar{K}_0^*(1430)^0$ and the nonresonant part], $P(\bar{K}^*(892)^0)$, $P'(\bar{K}^*(1410)^0)$, and $D(\bar{K}_2^*(1430)^0)$ components. The first and second uncertainties are statistical and systematic, respectively.

Variable	$S+P$	$S+P+P'$	$S+P+D$
$r_S(\mathrm{GeV})^{-1}$	$-11.57 \pm 0.58 \pm 0.46$	$-11.57 \pm 0.61 \pm 0.44$	$-11.94 \pm 0.58 \pm 0.50$
$r_S^{(1)}$	$0.08 \pm 0.05 \pm 0.05$	$0.08 \pm 0.05 \pm 0.05$	$0.03 \pm 0.05 \pm 0.07$
$a_{\mathrm{S,BG}}^{1/2}(\mathrm{GeV}/c)^{-1}$	$1.94 \pm 0.21 \pm 0.29$	$1.93 \pm 0.16 \pm 0.50$	$1.84 \pm 0.10 \pm 0.47$
$b_{\mathrm{S,BG}}^{1/2}(\mathrm{GeV}/c)^{-1}$	$-0.81 \pm 0.82 \pm 1.24$	-0.81 fixed	-0.81 fixed
$m_{\bar{K}^*(892)^0}(\mathrm{MeV}/c^2)$	$894.60 \pm 0.25 \pm 0.08$	$894.61 \pm 0.35 \pm 0.12$	$894.68 \pm 0.25 \pm 0.05$
$\Gamma^0_{\bar{K}^*(892)^0}(\mathrm{MeV}/c^2)$	$46.42 \pm 0.56 \pm 0.15$	$46.44 \pm 0.70 \pm 0.26$	$46.53 \pm 0.56 \pm 0.31$
$r_{\mathrm{BW}}(\mathrm{GeV}/c)^{-1}$	$3.07 \pm 0.26 \pm 0.11$	$3.05 \pm 0.61 \pm 0.30$	$3.01 \pm 0.26 \pm 0.22$
$m_V(\mathrm{GeV}/c^2)$	$1.81^{+0.25}_{-0.17} \pm 0.02$	$1.81^{+0.25}_{-0.17} \pm 0.02$	$1.80^{+0.24}_{-0.16} \pm 0.05$
$m_A(\mathrm{GeV}/c^2)$	$2.61^{+0.22}_{-0.17} \pm 0.03$	$2.60^{+0.22}_{-0.17} \pm 0.03$	$2.60^{+0.21}_{-0.17} \pm 0.04$
r_V	$1.411 \pm 0.058 \pm 0.007$	$1.410 \pm 0.057 \pm 0.006$	$1.406 \pm 0.058 \pm 0.022$
r_2	$0.788 \pm 0.042 \pm 0.008$	$0.788 \pm 0.041 \pm 0.008$	$0.784 \pm 0.041 \pm 0.024$
$r_{\bar{K}^*(1410)^0}$		$0.00 \pm 0.40 \pm 0.04$	
$\delta_{\bar{K}^*(1410)^0}(\mathrm{degree})$		0 fixed	
$r_{\bar{K}_2^*(1430)^0}(\mathrm{GeV})^{-4}$			$11.22 \pm 1.89 \pm 4.10$
$\delta_{\bar{K}_2^*(1430)^0}(\mathrm{degree})$			0 fixed
$f_S(\%)$	$6.05 \pm 0.22 \pm 0.18$	$6.06 \pm 0.24 \pm 0.18$	$5.90 \pm 0.23 \pm 0.20$
$f_{\bar{K}^*(892)^0}(\%)$	$93.93 \pm 0.22 \pm 0.18$	$93.91 \pm 0.24 \pm 0.18$	$94.00 \pm 0.23 \pm 0.16$
$f_{\bar{K}^*(1410)^0}(\%)$		$0 \pm 0.010 \pm 0.009$	
$f_{\bar{K}_2^*(1430)^0}(\%)$			$0.094 \pm 0.030 \pm 0.061$
χ^2/n.d.f.	292.7/291	292.7/291	292.7/292

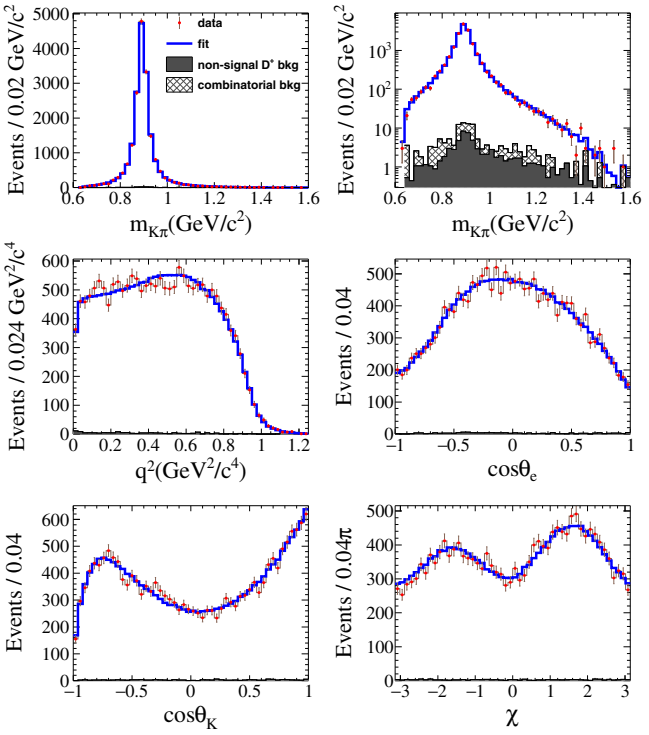

FIG. 4. Projections onto each of the kinematic variables, comparing data (dots with error bars) and signal MC determined by the PWA solution (solid line), assuming that the signal is composed of the S wave and the $\bar{K}^*(892)^0$. The shadowed histogram shows the nonsignal D^+ background estimated from MC simulation, and the hatched area shows the combinatorial background estimated from the $M_{\rm BC}$ sideband of data.

The fit results are summarized in the third and fourth columns of Table II. The contribution from the $\bar{K}^*(1410)^0$ is found to be consistent with zero when fixing $\delta_{\bar{K}^*(1410)^0}$ either at zero or π, while the $\bar{K}_2^*(1430)^0$ has a significance of 4.3σ, favoring $\delta_{\bar{K}_2^*(1430)^0}$ at zero. The upper limits of their branching fractions at 90% confidence level (C.L.) are calculated using a Bayesian approach. They are determined as the branching fraction below which lies 90% of the total likelihood integral in the positive branching fraction domain, assuming a uniform prior. To take the systematic uncertainty into account, the likelihood is convolved with a Gaussian function with a width equal to the systematic uncertainty. The branching fractions and their upper limits are measured to be

$$\begin{aligned}\mathcal{B}(D^+ \to \bar{K}^*(1410)^0 e^+\nu_e) &= (0 \pm 0.009 \pm 0.008)\%,\\ &< 0.028\%\ (90\%\ \text{C.L.}).\\ \mathcal{B}(D^+ \to \bar{K}_2^*(1430)^0 e^+\nu_e) &= (0.011 \pm 0.003 \pm 0.007)\%,\\ &< 0.023\%\ (90\%\ \text{C.L.}). \qquad (29)\end{aligned}$$

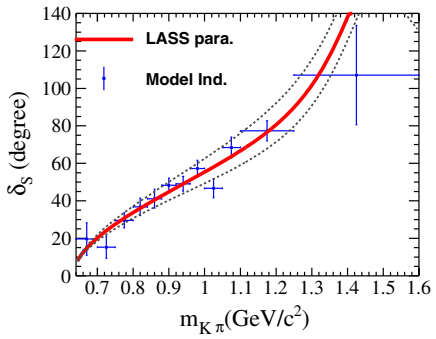

FIG. 5. Variation of the S-wave phase vs $m_{K\pi}$, assuming that the signal is composed of the S wave and the $\bar{K}^*(892)^0$. The points with error bars correspond to the model-independent measurement by fitting data; the solid line corresponds to the result based on the LASS parametrization: $a_{\rm B,SG}^{1/2} = 1.94$, $b_{\rm B,SG}^{1/2} = -0.81$; the dotted line shows the 1σ confidence band by combining the statistical and systematic errors in quadrature.

We also try to add both the $\bar{K}^*(1410)^0$ and $\bar{K}_2^*(1430)^0$ to the fit, obtaining results that are quite close to the solution in the fourth column of Table II. This suggests that the $\bar{K}^*(1410)^0$ contribution can be neglected.

In the PWA fit, only the ratios of the transition form factors r_V and r_2 are measured. Given the result of $\mathcal{B}(D^+ \to \bar{K}^*(892)^0 e^+\nu_e)$ from Eq. (28), we can calculate the $A_1(0)$ value and thus obtain the absolute values of the form factors, which can be compared with the lattice QCD determinations.

The value of $A_1(0)$ is calculated by comparing the absolute branching fraction and the integration of the differential decay rate given in Eq. (4) over the five-dimensional space for the $D^+ \to \bar{K}^*(892)^0 e^+\nu_e$ process. Restricting Eq. (4) to the $\bar{K}^*(892)^0$ contribution only and integrating it over the three angles, we obtain

$$\frac{d\Gamma}{dq^2 dm^2} = \frac{1}{3}\frac{G_F^2|V_{cs}|^2}{(4\pi)^5 m_D^2}\beta p_{K\pi}\left[\frac{2}{3}\{|\mathcal{F}_{11}|^2 + |\mathcal{F}_{21}|^2 + |\mathcal{F}_{31}|^2\}\right]. \qquad (30)$$

Assuming that $\bar{K}^*(892)^0$ has an infinitesimal width and a single pole mass of 894.60 MeV/c^2, and integrating Eq. (30) over q^2, we find

$$\begin{aligned}\Gamma &= \frac{G_F^2|V_{cs}|^2}{96\pi^3 m_D^2}\frac{2}{3}|A_1(0)|^2\mathbb{X}\\ &\equiv \frac{\hbar\mathcal{B}(D^+ \to \bar{K}^*(892)^0 e^+\nu_e)\mathcal{B}(\bar{K}^*(892)^0 \to K^-\pi^+)}{\tau_{D^+}} \qquad (31)\end{aligned}$$

with

$$\mathbb{X} = \int_0^{q^2_{\rm max}} p_{K\pi} q^2 \frac{|H_0|^2 + |H_+|^2 + |H_-|^2}{|A_1(0)|^2} dq^2.$$

Here, $\hbar$ is the reduced Planck constant, and τ_{D^+} is the lifetime of the D^+ meson. The integral $\mathbb{X}$ is evaluated

TABLE III. Systematic uncertainties of the PWA nominal solution arsing from: (I) the background fraction, (II) the background shape, (III) the $\bar{K}_0^*(1430)^0$ mass and width, (IV) additional resonances, (V) the tracking efficiency correction, and (VI) the PID efficiency correction.

Variable	I	II	III	IV	V	VI	Total
$\Delta r_S(\mathrm{GeV})^{-1}$	0.03	0.26	0.10	0.37	0.01	0.01	0.46
$\Delta r_S^{(1)}$	0.00	0.02	0.01	0.05	0.00	0.00	0.05
$\Delta a_{\mathrm{S,BG}}^{1/2}(\mathrm{GeV}/c)^{-1}$	0.01	0.04	0.27	0.10	0.01	0.00	0.29
$\Delta b_{\mathrm{S,BG}}^{1/2}(\mathrm{GeV}/c)^{-1}$	0.03	0.21	1.20	0.23	0.02	0.00	1.24
$\Delta m_{\bar{K}^*(892)^0}(\mathrm{MeV}/c^2)$	0.00	0.02	0.00	0.07	0.00	0.00	0.08
$\Delta\Gamma^0_{\bar{K}^*(892)^0}(\mathrm{MeV}/c^2)$	0.01	0.10	0.02	0.11	0.00	0.00	0.15
$\Delta r_{\mathrm{BW}}(\mathrm{GeV}/c)^{-1}$	0.00	0.09	0.02	0.06	0.00	0.00	0.11
$\Delta m_V(\mathrm{GeV}/c^2)$	0.00	0.01	0.00	0.02	0.01	0.00	0.02
$\Delta m_A(\mathrm{GeV}/c^2)$	0.00	0.02	0.00	0.01	0.01	0.00	0.03
Δr_V	0.001	0.004	0.001	0.005	0.001	0.001	0.007
Δr_2	0.000	0.005	0.001	0.004	0.005	0.000	0.008

using r_2, r_V, m_V, and m_A from the PWA solution. Using the values $\tau_{D^+} = (10.40 \pm 0.07) \times 10^{-13}$ s and $|V_{cs}| = 0.986 \pm 0.016$ from PDG, one gets

$$A_1(0) = 0.589 \pm 0.010 \pm 0.012. \tag{32}$$

This result is more than one standard deviation lower than that in Ref. [3]. The difference can mostly be explained by the lower value of $\mathcal{B}(D^+ \to \bar{K}^*(892)^0 e^+ \nu_e)$ in Eq. (28) and by the renewed measurement of $|V_{cs}|$ in the PDG.

If, instead of approximating the $\bar{K}^*(892)^0$ mass distribution as a delta function, we use the fitted mass distribution of the resonance to integrate the differential decay rate over q^2 and m^2, the result becomes

$$A_1(0)|_{q^2,m^2} = 0.619 \pm 0.011 \pm 0.013, \tag{33}$$

where the integration for m^2 is performed over the mass range $0.6 < m_{K\pi} < 1.6\ \mathrm{GeV}/c^2$. We do not observe the large difference between $A_1(0)$ and $A_1(0)|_{q^2,m^2}$ reported in Ref. [3].

In PWA, the systematic uncertainty of each parameter is defined as the difference between the fit result in the nominal condition and that obtained after some condition is varied corresponding to one source of uncertainty. Systematic uncertainties of the nominal solution are summarized in Table III. The uncertainty due to the background fraction is estimated by varying the background fraction by 1σ in the same way as when estimating this uncertainty in the branching fraction measurement in Sec. III. Uncertainties due to the assumed shapes of the backgrounds are considered separately for the combinatorial background and the nonsignal D^+ decays. The former is estimated by varying the M_{BC} sideband, while for the latter, only the uncertainty from $D^+ \to K^-\pi^+\pi^+\pi^0$ is considered, which is estimated by comparing the difference between two extreme cases: the phase space process and $D^+ \to \bar{K}^*(892)^0\rho^+$. The uncertainty due to the shape of the other nonsignal D^+ decays can be neglected. The uncertainty arising from the fixed mass and width of the $\bar{K}_0^*(1430)^0$ is considered by varying their values by 1σ according to the PDG. To estimate the uncertainty caused by the additional resonances, we compare different solutions in Table II and take the largest differences between them as systematic uncertainties. $b_{S,\mathrm{BG}}^{1/2}$ has been fixed in solutions with the $\bar{K}^*(1410)^0$ or $\bar{K}_2^*(1430)^0$ component considered. We then allow it to be a free parameter in the fits, and the largest variation of $b_{S,\mathrm{BG}}^{1/2}$ is taken as the uncertainty. The uncertainty associated with the efficiency correction of tracking and particle identification is obtained by varying the correction factor by 1σ. The possible uncertainty due to the fit procedure is studied with 500 fully reconstructed data-sized signal MC samples generated according to the PWA result. The input-output check shows that biases of all the fit parameters are negligible. Assuming that all the uncertainties described above are independent of each other, we add them in quadrature to obtain the total. In a similar way, systematic uncertainties on the S-wave phase δ_S are estimated and presented in Table IV.

V. DETERMINATION OF HELICITY BASIS FORM FACTORS

In the K^*-dominated region, the contribution of non-$\bar{K}^*(892)^0$ resonances is negligible, and the decay intensity can be parametrized by helicity basis form factors $H_{\pm,0}(q^2, m^2)$ describing the decay into the $\bar{K}^*(892)^0$ vector and by an additional form factor $h_0(q^2, m^2)$ describing the nonresonant S-wave contribution. This allows us to transform the matrix element $\mathcal{I}$ in Eq. (4) into a simplified form [24]. By performing an integration over the acoplanarity angle χ and neglecting the terms suppressed by the factor m_e^2/q^2, one obtains

TABLE IV. The S-wave phase δ_S measured in the 12 $m_{K\pi}$ bins with statistical and systematic uncertainties. The systematic uncertainties include: (I) the background fraction, (II) the background shape, (III) the $\bar{K}_0^*(1430)^0$ mass and width, (IV) additional resonances, (V) the tracking efficiency correction, (VI) the PID efficiency correction.

$m_{K\pi}$ bin (GeV/c^2)	Value (degrees)	Statistical (degrees)	Systematic						
			I	II	III	IV	V	VI	Total
0.60–0.70	19.63	8.58	0.08	0.42	1.10	0.52	0.19	0.10	1.31
0.70–0.75	15.22	5.51	0.02	2.20	0.05	0.09	0.02	0.01	2.20
0.75–0.80	29.55	3.93	0.16	0.21	0.12	0.50	0.10	0.10	0.60
0.80–0.84	36.74	4.61	0.00	0.25	0.23	0.27	0.04	0.04	0.44
0.84–0.88	41.10	4.96	0.03	0.31	0.23	0.70	0.06	0.06	0.80
0.88–0.92	48.28	3.71	0.04	0.22	0.13	0.46	0.04	0.04	0.53
0.92–0.96	49.06	3.76	0.03	0.54	0.12	1.10	0.01	0.01	1.23
0.96–1.00	57.27	4.15	0.04	0.28	0.19	1.30	0.05	0.05	1.35
1.00–1.05	46.63	4.47	0.01	0.25	0.34	2.30	0.18	0.18	2.35
1.05–1.10	68.46	5.01	0.01	1.10	0.18	2.10	0.03	0.03	2.38
1.10–1.25	77.32	4.34	0.18	1.20	1.30	2.80	0.13	0.12	3.32
1.25–1.60	107.08	11.24	0.97	10.00	9.50	20.00	1.10	1.10	24.36

$$\int \mathcal{I} d\chi = \frac{q^2 - m_e^2}{8} \times \left\{ \begin{array}{c} ((1+\cos\theta_e)\sin\theta_K)^2 |H_+(q^2,m^2)|^2 |A_{K^*}(m)|^2 \\ +((1-\cos\theta_e)\sin\theta_K)^2 |H_-(q^2,m^2)|^2 |A_{K^*}(m)|^2 \\ +(2\sin\theta_e\cos\theta_K)^2 |H_0(q^2,m^2)|^2 |A_{K^*}(m)|^2 \\ \underline{+8\sin^2\theta_e\cos\theta_K H_0(q^2,m^2) h_0(q^2,m^2)}\ \underline{\mathrm{Re}\{A_S e^{-i\delta_S} A_{K^*}(m)\}} \\ \underline{+4\sin^2\theta_e A_S^2 |h_0(q^2,m^2)|^2} \end{array} \right\}. \tag{34}$$

Here, $A_{K^*}(m)$ denotes the $\bar{K}^*(892)^0$ amplitude,

$$A_{K^*}(m) = \frac{\sqrt{m_0\Gamma_0}\left(\frac{p^*(m)}{p^*(m_0)}\right)}{m^2 - m_0^2 + i m_0 \Gamma_0 \left(\frac{p^*(m)}{p^*(m_0)}\right)^3}, \tag{35}$$

where m_0 and Γ_0 are the mass and the width of $\bar{K}^*(892)^0$ with their values taken from the second column of Table II.

The underlined terms in Eq. (34) represent the nonresonant S-wave contribution which was described for the first time in Ref. [2]. The mass and q^2 dependence of the nonresonant S-wave amplitude is parametrized as $h_0(q^2,m^2)A_S(m)e^{i\delta_S(m)}$, where the form factor $h_0(q^2,m^2)$ is not assumed to be the same as $H_0(q^2,m^2)$. Generally, both the amplitude modulus $A_S(m)$ and the phase $\delta_S(m)$ are mass dependent. However, in this section, $A_S(m)$ and $\delta_S(m)$ are both assumed to be constant throughout the K^*-dominated mass region. The value of $\delta_S = 39°$ is taken from Ref. [6].

The helicity basis form-factor products $|H_+(q^2,m^2)|^2$, $|H_-(q^2,m^2)|^2$, $|H_0(q^2,m^2)|^2$, $A_S H_0(q^2,m^2)h_0(q^2,m^2)$, and $A_S^2 h_0^2(q^2,m^2)$ in Eq. (34), which we denote with $\alpha = \{+,-,0,I,S\}$ correspondingly, can be extracted from the angular distributions in Eq. (34) in a model-independent way using the projective weighting technique, which was introduced in Ref. [24].

In general, the form-factor products are functions of q^2 and m^2. However, in this work, we measure the average values over the relatively narrow K^*-dominated region. Taking $|H_+(q^2,m^2)|^2$, for example,

$$|H_+(q^2)|^2 = \frac{\int |H_+(q^2,m^2)|^2 F(q^2,m^2) |A_{K^*}(m)|^2 dm^2}{\int F(q^2,m^2)|A_{K^*}(m)|^2 dm^2}, \tag{36}$$

where the integration is performed over the mass range $0.8 < m < 1.0\ \mathrm{GeV}/c^2$. The kinematic factor $F(q^2,m^2)$ is defined as

$$F(q^2,m^2) = \frac{(q^2 - m_e^2) p_{K\pi} p^*}{mq}, \tag{37}$$

where $p_{K\pi}$ and p^* are defined in Sec. IV. Similarly, this averaging procedure is also performed for the other form-factor products.

To obtain the form-factor product dependence on q^2, we divide the q^2 range $0 < q^2 < 1.0\ \mathrm{GeV}^2/c^4$ into ten equal bins. The form-factor products are to be calculated in each

TABLE V. Average form-factor products in the K^*-dominated region. The first and second uncertainties are statistical and systematic, respectively.

q^2 (GeV$^2/c^4$)	$H_+^2(q^2)$	$H_-^2(q^2)$	$q^2H_0^2(q^2)$	$A_s q^2 H_0(q^2)h_0(q^2)$	$A_s^2 q^2 h_0^2(q^2)$
0.0–0.1	$1.67 \pm 0.46 \pm 0.12$	$0.92 \pm 1.71 \pm 0.31$	$0.89 \pm 0.05 \pm 0.02$	$0.52 \pm 0.08 \pm 0.06$	$0.09 \pm 0.23 \pm 0.05$
0.1–0.2	$0.12 \pm 0.13 \pm 0.05$	$1.26 \pm 0.50 \pm 0.12$	$1.02 \pm 0.05 \pm 0.02$	$0.57 \pm 0.09 \pm 0.05$	$0.38 \pm 0.21 \pm 0.05$
0.2–0.3	$0.39 \pm 0.10 \pm 0.03$	$2.39 \pm 0.33 \pm 0.13$	$1.14 \pm 0.06 \pm 0.02$	$0.69 \pm 0.10 \pm 0.05$	$-0.24 \pm 0.24 \pm 0.11$
0.3–0.4	$0.41 \pm 0.07 \pm 0.03$	$1.99 \pm 0.20 \pm 0.07$	$0.99 \pm 0.06 \pm 0.03$	$0.36 \pm 0.10 \pm 0.07$	$-0.04 \pm 0.23 \pm 0.10$
0.4–0.5	$0.26 \pm 0.06 \pm 0.03$	$1.64 \pm 0.13 \pm 0.06$	$0.89 \pm 0.06 \pm 0.04$	$0.41 \pm 0.11 \pm 0.06$	$0.48 \pm 0.22 \pm 0.14$
0.5–0.6	$0.41 \pm 0.06 \pm 0.05$	$1.81 \pm 0.11 \pm 0.07$	$0.93 \pm 0.07 \pm 0.05$	$0.20 \pm 0.12 \pm 0.07$	$0.14 \pm 0.27 \pm 0.18$
0.6–0.7	$0.49 \pm 0.06 \pm 0.03$	$1.60 \pm 0.10 \pm 0.07$	$0.92 \pm 0.08 \pm 0.05$	$0.39 \pm 0.14 \pm 0.09$	$0.25 \pm 0.31 \pm 0.22$
0.7–0.8	$0.51 \pm 0.06 \pm 0.05$	$1.64 \pm 0.10 \pm 0.12$	$1.15 \pm 0.10 \pm 0.09$	$0.36 \pm 0.15 \pm 0.11$	$0.06 \pm 0.39 \pm 0.27$
0.8–0.9	$0.72 \pm 0.08 \pm 0.08$	$1.49 \pm 0.11 \pm 0.15$	$1.17 \pm 0.11 \pm 0.15$	$0.17 \pm 0.14 \pm 0.10$	$0.02 \pm 0.56 \pm 0.42$
0.9–1.0	$0.56 \pm 0.13 \pm 0.01$	$1.10 \pm 0.15 \pm 0.05$	$0.89 \pm 0.18 \pm 0.11$	$0.10 \pm 0.14 \pm 0.03$	$1.33 \pm 0.67 \pm 0.33$

q^2 bin independently. For events in a given q^2 bin, we consider 100 two-dimensional $\Delta\cos\theta_K \times \Delta\cos\theta_e$ angular bins: ten equal-size bins in $\cos\theta_K$ times ten equal-size bins in $\cos\theta_e$. Each event is assigned a weight to project out the given form-factor product depending on the angular bin it is reconstructed in.

Such a weighting is equivalent to calculating a scalar product $\vec{P}_\alpha \cdot \vec{D}$. Here, $\vec{D} = \{n_1 n_2 \ldots n_{100}\}$ is a data vector of the observed angular bin populations of which the jth component is the number of data events n_j in the jth angular bin, $j = 1, 2 \ldots 100$. $\vec{P}_\alpha$ is a projection vector for the form-factor product α, the components of which serve as weights applied to the events in a given angular bin. Calculating the scalar product $\vec{P}_\alpha \cdot \vec{D}$ is equivalent to weighting events in the first angular bin by $[\vec{P}_\alpha]_1$, in the second bin by $[\vec{P}_\alpha]_2$, etc.:

$$\vec{P}_\alpha \cdot \vec{D} = [\vec{P}_\alpha]_1 n_1 + [\vec{P}_\alpha]_2 n_2 + \cdots + [\vec{P}_\alpha]_{100} n_{100}. \quad (38)$$

The weight vector $\vec{P}_\alpha$ and the scalar product $\vec{P}_\alpha \cdot \vec{D}$ can be calculated following the idea described below. First, the data vector $\vec{D}$ can be written as a sum of contributions from the terms related to the individual form-factor products in Eq. (34):

$$\begin{aligned}\vec{D} &= f_+\vec{m}_+ + f_-\vec{m}_- + f_0\vec{m}_0 + f_I\vec{m}_I + f_S\vec{m}_S \\ &= \sum_\alpha f_\alpha \vec{m}_\alpha. \end{aligned} \quad (39)$$

Here, the vectors $\vec{m}_\alpha$ represent the angular distributions of the contributions from the individual form-factor product components of Eq. (34) into $\vec{D}$. They are obtained based on MC simulation which will be discussed later. The coefficients f_α represent the relative ratio of the individual contributions, which are proportional to the corresponding form-factor products.

If we define a 5×100 matrix M as

$$M = (\,\vec{m}_+ \quad \vec{m}_- \quad \vec{m}_0 \quad \vec{m}_I \quad \vec{m}_S\,)^T, \quad (40)$$

Eq. (39) can be transformed into

$$\begin{pmatrix} \vec{m}_+ \cdot \vec{D} \\ \vec{m}_- \cdot \vec{D} \\ \vec{m}_0 \cdot \vec{D} \\ \vec{m}_I \cdot \vec{D} \\ \vec{m}_S \cdot \vec{D} \end{pmatrix} = MM^T \begin{pmatrix} f_+ \\ f_- \\ f_0 \\ f_I \\ f_S \end{pmatrix}. \quad (41)$$

The solution of Eq. (41) is

$$(\,f_+ \quad f_- \quad f_0 \quad f_I \quad f_S\,)^T = P\vec{D}, \quad (42)$$

with the weight matrix P defined by

$$P = (\,\vec{P}_+ \quad \vec{P}_- \quad \vec{P}_0 \quad \vec{P}_I \quad \vec{P}_S\,)^T = (MM^T)^{-1}M, \quad (43)$$

the component $[\vec{P}_\alpha]_k$ of which is used as the weight for the construction of the form-factor product α in the kth angular bin.

The matrix M is obtained by weighting the PHSP signal MC. The simulated events pass the usual procedure of detector simulation and event selection, allowing correction for the biases due to the finite detector resolution and selection efficiency. Each of the $\vec{m}_\alpha$ vectors is calculated by weighing the PHSP sample so that the resulting data reproduces the distribution of Eq. (34) with the form-factor product α set at 1 and all the others being equal to zero. For a given event of θ_e, θ_K, m^2, and q^2, the following weights are assigned to calculate the corresponding $\vec{m}_\alpha$ vector:

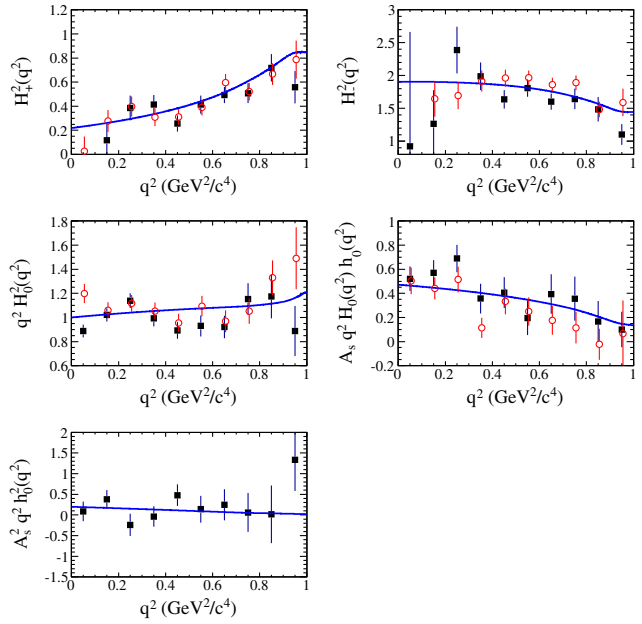

FIG. 6. Average form-factor products in the K^*-dominated region. The model-independent measurements in this work (squares) are compared with the CLEO-c results (circles) and with our PWA solution (curves). In the CLEO-c results, 0.33 GeV^{-1} is taken as the A_S value for comparison [6]. Error bars represent statistical and systematic uncertainties combined in quadrature.

$$\begin{aligned}
\omega_+ &= F(q^2,m^2)|A_{K^*}(m)|^2((1+\cos\theta_e)\sin\theta_K)^2,\\
\omega_- &= F(q^2,m^2)|A_{K^*}(m)|^2((1-\cos\theta_e)\sin\theta_K)^2,\\
\omega_0 &= F(q^2,m^2)|A_{K^*}(m)|^2(2\sin\theta_e\cos\theta_K)^2,\\
\omega_I &= 8F(q^2,m^2)\mathrm{Re}\{e^{-i\delta_S}A_{K^*}(m)\}\sin^2\theta_e\cos\theta_K,\\
\omega_S &= 4F(q^2,m^2)\sin^2\theta_e. \qquad (44)
\end{aligned}$$

Given the matrix M determined by MC simulation, the weight matrix P can be calculated using Eq. (43), and the form-factor products can be obtained by applying P to the data vector $\vec{D}$ according to Eq. (42). This procedure is performed to calculate the form-factor products for each q^2 bin independently. The correlation between the q^2 bins is negligible due to the excellent q^2 resolution.

The procedure described above provides the form-factor products with an arbitrary normalization factor common for all of them. In this work, we use the normalization $q^2|H_0(q^2)|^2 \to 1$ when $q^2 \to 0$.

In total, 16181 $D^+ \to K^-\pi^+e^+\nu_e$ candidates are selected in the K^*-dominated region. The influence of the small residual background on the results is insignificant. To avoid numerical instability caused by negative bin content after background subtraction, the final results presented in Table V are obtained neglecting the background contribution.

In Fig. 6, the results are compared with the CLEO-c results [25] and with our PWA solution. The model-independent measurements are consistent with the SPD model with the parameters determined by the PWA fit. They are also consistent with the results previously reported by CLEO-c.

The systematic uncertainties of the form-factor product determination originate mostly from the $\vec{m}_\alpha$ calculation. They are estimated using a large generator-level PHSP sample, with which the form-factor products are computed using the generator-level kinematic variables. The difference between the input and the computed value is taken as the systematic uncertainty related to the $\vec{m}_\alpha$ calculation procedure. The limited statistics of PHSP signal MC used to calculate the $\vec{m}_\alpha$ vectors is another source of uncertainty. To estimate its contribution, we randomly select subsamples from the generator-level PHSP sample with roughly the size of the PHSP signal MC. The standard deviation of the form-factor products computed using the different subsamples is taken as the systematic uncertainty. The uncertainties due to neglecting the residual background as well as from other sources are negligible. The main systematic uncertainties are presented in Table VI.

VI. SUMMARY

An analysis of $D^+ \to K^-\pi^+e^+\nu_e$ has been performed, and its branching fraction has been measured over the full $m_{K\pi}$ range ($0.6 < m_{K\pi} < 1.6$ GeV/c^2) and in the K^*-dominated region ($0.8 < m_{K\pi} < 1.0$ GeV/c^2).

Using a PWA fit, we analyzed the components in the $D^+ \to K^-\pi^+e^+\nu_e$ decay. In addition to the process $D^+ \to \bar{K}^*(892)^0e^+\nu_e$, we observed the $K\pi$ S-wave component with a fraction of $(6.05 \pm 0.22 \pm 0.18)\%$. Possible contributions from the $\bar{K}^*(1410)^0$ and $\bar{K}_2^*(1430)^0$ were observed to have significances less than 5σ, and the upper limits were provided.

With the signal including the S wave and $\bar{K}^*(892)^0$ as the nominal fit, the form factors based on the SPD model, together with the parameters describing the $\bar{K}^*(892)^0$, were measured. We performed the first measurement of the vector pole mass m_V in this decay, $m_V = 1.81^{+0.25}_{-0.17} \pm 0.02$ GeV/c^2. In the channel $D^0 \to K^-e^+\nu_e$, the value $m_V = 1.884 \pm 0.012 \pm 0.014$ GeV/c^2 was obtained [26]. When we fixed m_V at 2.0 GeV/c^2 as in Ref. [3], consistent results for the form factor parameters were obtained, as shown in Table VII.

We measured the S-wave phase variation with $m_{K\pi}$ in a model-independent way and found an agreement with the PWA solution based on the parametrization in the LASS scattering experiment.

Finally, we performed a model-independent measurement of the q^2 dependence of the helicity basis form factors. It agreed well with the CLEO-c result and the PWA solution based on the SPD model.

TABLE VI. Systematic uncertainties of the form-factor products: the first numbers are uncertainties due to the limited PHSP sample size, while the second represent uncertainties due to the $\vec{m}_\alpha$ calculation.

q^2 (GeV$^2/c^4$)	$H_+^2(q^2)$		$H_-^2(q^2)$		$q^2H_0^2(q^2)$		$A_s q^2 H_0(q^2)h_0(q^2)$		$A_s^2 q^2 h_0^2(q^2)$	
0.0–0.1	0.11	0.05	0.14	0.27	0.02	0.00	0.05	0.03	0.04	0.02
0.1–0.2	0.05	0.03	0.07	0.10	0.02	0.00	0.05	0.01	0.05	0.01
0.2–0.3	0.03	0.01	0.06	0.11	0.02	0.00	0.05	0.00	0.07	0.08
0.3–0.4	0.03	0.01	0.06	0.05	0.03	0.02	0.06	0.03	0.09	0.05
0.4–0.5	0.03	0.01	0.06	0.02	0.03	0.02	0.06	0.01	0.12	0.06
0.5–0.6	0.03	0.03	0.07	0.01	0.05	0.03	0.07	0.02	0.17	0.06
0.6–0.7	0.03	0.01	0.06	0.04	0.05	0.03	0.08	0.04	0.17	0.14
0.7–0.8	0.04	0.04	0.08	0.08	0.05	0.07	0.08	0.07	0.26	0.02
0.8–0.9	0.06	0.05	0.10	0.11	0.08	0.12	0.09	0.03	0.41	0.03
0.9–1.0	0.01	0.01	0.01	0.05	0.01	0.11	0.01	0.03	0.04	0.33

TABLE VII. Form-factor parameter results with m_V allowed to vary or fixed at 2.0 GeV$/c^2$. The first and second uncertainties are statistical and systematic, respectively. When m_V is fixed, the m_V induced uncertainty is especially considered by varying m_V from 1.7 to 2.2 GeV$/c^2$ besides the ones listed in Table III.

Variable	m_V allowed to vary	m_V fixed
m_V (GeV$/c^2$)	$1.81^{+0.25}_{-0.17} \pm 0.02$	2.0
m_A (GeV$/c^2$)	$2.61^{+0.22}_{-0.17} \pm 0.03$	$2.64^{+0.22}_{-0.17} \pm 0.07$
r_V	$1.411 \pm 0.058 \pm 0.007$	$1.449 \pm 0.034 \pm 0.071$
r_2	$0.788 \pm 0.042 \pm 0.008$	$0.795 \pm 0.040 \pm 0.016$
$A_1(0)$	$0.589 \pm 0.010 \pm 0.012$	$0.589 \pm 0.010 \pm 0.014$

ACKNOWLEDGMENTS

The BESIII Collaboration thanks the staff of Beijing Electron-Positron Collider II and the IHEP computing center for their strong support. This work is supported in part by National Key Basic Research Program of China under Contracts No. 2009CB825204 and No. 2015CB856700; National Natural Science Foundation of China (NSFC) under Contracts No. 10935007, No. 11075174, No. 11121092, No. 11235011, No. 11125525, No. 11322544, No. 11335008, No. 11425524, and No. 11475185; the Chinese Academy of Sciences (CAS) Large-Scale Scientific Facility Program; the CAS Center for Excellence in Particle Physics; the Collaborative Innovation Center for Particles and Interactions; Joint Large-Scale Scientific Facility Funds of the NSFC and CAS under Contracts No. 11179007, No. U1232201, and No. U1332201; CAS under Contracts No. KJCX2-YW-N29 and No. KJCX2-YW-N45; 100 Talents Program of CAS; National 1000 Talents Program of China; INPAC and Shanghai Key Laboratory for Particle Physics and Cosmology; German Research Foundation DFG under Contract No. Collaborative Research Center CRC-1044; Istituto Nazionale di Fisica Nucleare, Italy; Ministry of Development of Turkey under Contract No. DPT2006K-120470; Russian Foundation for Basic Research under Contract No. 14-07-91152; The Swedish Resarch Council; U. S. Department of Energy under Contracts No. DE-FG02-04ER41291, No. DE-FG02-05ER41374, No. DE-SC0012069, and No. DESC0010118; U.S. National Science Foundation; University of Groningen and the Helmholtzzentrum fuer Schwerionenforschung GmbH, Darmstadt; WCU Program of National Research Foundation of Korea under Contract No. R32-2008-000-10155-0.

[1] C. W. Bernard, A. X. El-Khadra, and A. Soni, Phys. Rev. D **45**, 869 (1992); V. Lubicz, G. Martinelli, M. S. McCarthy, and C. T. Sachrajda, Phys. Lett. B **274**, 415 (1992); A. Abada *et al.*, Nucl. Phys. **B416**, 675 (1994); K. C. Bowler, N. M. Hazel, H. Hoeber, R. D. Kenway, D. G. Richards, L. Lellouch, J. Nieves, C. T. Sachrajda, and H. Wittig (UKQCD Collaboration), Phys. Rev. D **51**, 4905 (1995); T. Bhattacharya and R. Gupta, Nucl. Phys. B, Proc. Suppl. **47**, 481 (1996); C. R. Allton *et al.* (APE Collaboration), Phys. Lett. B **345**, 513 (1995); S. Gusken, G. Siegert, and K. Schilling, Prog. Theor. Phys. Suppl. **122**, 129 (1996); A. Abada, D. Becirevic, Ph. Boucaud, J. Flynn, J. P. Leroy, V. Lubicz, and F. Mescia (SPQcdR Collaboration), Nucl. Phys. B, Proc. Suppl. **119**, 625 (2003).

[2] J. M. Link *et al.* (FOCUS Collaboration), Phys. Lett. B **535**, 43 (2002).

[3] P. del Amo Sanchez *et al.* (*BABAR* Collaboration), Phys. Rev. D **83**, 072001 (2011).

[4] D. Aston *et al.*, Nucl. Phys. **B296**, 493 (1988).

[5] J. G. Korner and G. A. Schuler, Z. Phys. C **46**, 93 (1990); F. J. Gilman and R. L. Singleton, Jr., Phys. Rev. D **41**, 142 (1990).
[6] J. M. Link *et al.* (FOCUS Collaboration), Phys. Lett. B **544**, 89 (2002).
[7] M. Ablikim *et al.* (BESIII Collaboration), Chin. Phys. C **37**, 123001 (2013).
[8] M. Ablikim *et al.* (BESIII Collaboration), Phys. Lett. B **753**, 629 (2016).
[9] M. Ablikim *et al.*, Nucl. Instrum. Methods Phys. Res., Sect. A **614**, 345 (2010).
[10] S. Agostinelli *et al.* (GEANT4 Collaboration), Nucl. Instrum. Methods Phys. Res., Sect. A **506**, 250 (2003).
[11] S. Jadach, B. F. L. Ward, and Z. Was, Comput. Phys. Commun. **130**, 260 (2000); Phys. Rev. D **63**, 113009 (2001).
[12] D. J. Lange, Nucl. Instrum. Methods Phys. Res., Sect. A **462**, 152 (2001); R. G. Ping, Chin. Phys. C **32**, 599 (2008).
[13] E. Barberio and Z. Was, Comput. Phys. Commun. **79**, 291 (1994).
[14] K. A. Olive *et al.* (Particle Data Group Collaboration), Chin. Phys. C **38**, 090001 (2014).
[15] J. C. Chen, G. S. Huang, X. R. Qi, D. H. Zhang, and Y. S. Zhu, Phys. Rev. D **62**, 034003 (2000).
[16] R. M. Baltrusaitis *et al.*, Phys. Rev. Lett. **56**, 2140 (1986).
[17] H. Albrecht *et al.* (ARGUS Collaboration), Phys. Lett. B **241**, 278 (1990).
[18] N. Cabibbo and A. Maksymowicz, Phys. Rev. B **137**, B438 (1965).
[19] C. L. Y. Lee, M. Lu, and M. B. Wise, Phys. Rev. D **46**, 5040 (1992).
[20] K. M. Watson, Phys. Rev. **95**, 228 (1954).
[21] A. K. Leibovich, Z. Ligeti, I. W. Stewart, and M. B. Wise, Phys. Rev. D **57**, 308 (1998); J. Charles, A. Le Yaouanc, L. Oliver, O. Pene, and J. C. Raynal, Phys. Rev. D **60**, 014001 (1999); A. Datta, Y. Gao, A. V. Gritsan, D. London, M. Nagashima, and A. SzynkmanA. Datta, Y. Gao, A. V. Gritsan, D. London, M. Nagashima, and A. Szynkman, Phys. Rev. D **77**, 114025 (2008).
[22] F. James, Report No. CERN 68-15, 1968.
[23] J. M. Link *et al.* (FOCUS Collaboration), Phys. Lett. B **621**, 72 (2005).
[24] J. M. Link *et al.* (FOCUS Collaboration), Phys. Lett. B **633**, 183 (2006).
[25] R. A. Briere *et al.* (CLEO Collaboration), Phys. Rev. D **81**, 112001 (2010).
[26] B. Aubert *et al.* (*BABAR* Collaboration), Phys. Rev. D **76**, 052005 (2007).